Student thesis series INES nr 367

Quantification of a continuous-cover forest in Sweden using remote sensing techniques

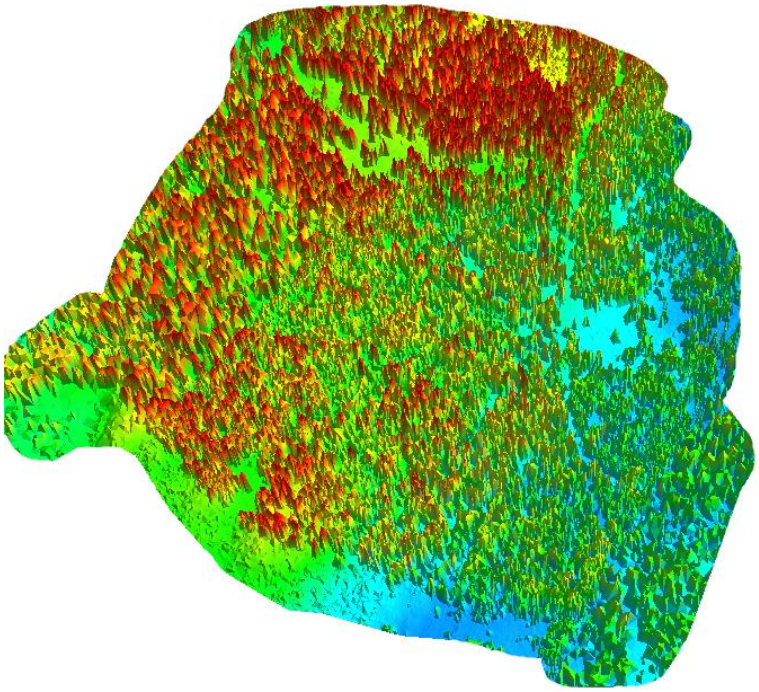

Johan Westin

2015

Department of

Physical Geography and Ecosystems Science

Lund University

Sölvegatan 12

S-223 62 Lund

Sweden

Johan Westin (2015). ***Quantification of a continuous-cover forest in Sweden using remote sensing techniques***

Master degree thesis, 30 ECTS credits in *Physical Geography and Ecosystem Analysis*

Department of Physical Geography and Ecosystems Science, Lund University

Level: Master of Science (MSc)

Course duration: *January* 2015 until *June* 2015

Disclaimer:

Cover image: 3D Subset of the digital surface model covering the Romperöd forest (visualized in Mars Explorer software).

Quantification of a continuous-cover forest in Sweden using remote sensing techniques

---

Johan Westin

Master thesis, 30 credits, in *Physical Geography and Ecosystem Analysis*

Supervisors:
Niklas Boke-Olén, PhD Student
Patrik Vestin, PhD Student

Exam committee:
Jonas Ardö, PhD Senior lecturer
Fredrik Lagergren, PhD Researcher

Department of Physical Geography and Ecosystem Science
Lund University

Abstract

Quantifying forest information about e.g. land cover, tree height and biomass has traditionally been a both time-consuming and labor-intensive part of forestry and forest research as field measurements typically are collected manually using handheld equipment. Remote sensing has proved to be a valuable complement to field based measurements as it enables for fast and relatively cheap collection of data from areas that would be hard to access from the ground. The aim of this thesis was to map and quantify the Romperöd forest located outside Glimåkra in southern Sweden. The forest has been managed using selective thinning forestry since the 1960's and surrounds a tower where micrometeorological measurements are being collected as a part of a research project aiming to study the effects different forestry practices have on the greenhouse gas balance of forests. The study was carried out using high resolution multispectral aerial images and small-footprint LiDAR remote sensing data included in the national elevation model in conjunction with field measurements. The results revealed a mixed forest where Norway spruce is the most dominating tree species, accounting for 40.2 % of the total coverage of the study area, followed by Scots pine (13.8 %), broadleaved trees (8.7 %), succession (6.7 %) and bare-ground (4.1 %). The object-based land cover classification outperformed the pixel-based approach, demonstrating the importance of spectral, textural and spatial information when classifying high resolution data over complex study areas, like a heterogeneous forest. The elevation of the terrain varies between 76.2 and 107.3 meters above sea level, with a ridge extending from south to north. The canopy height of the forest varies greatly throughout the study area and ranged between 1.0 and 34.6 m with an average height of 15.1 m and a standard deviation of 8 m. Above ground biomass (AGB) was modelled using a combination of LiDAR data and field measurements and showed an average AGB of 122 900 kg/ha and a standard deviation of 50 497 kg/ha. The model managed to explain 70 % of the variability in the field measured AGB estimates. The results were compared to the AGB data included in the SLU Forest Map which showed low correlation with AGB estimates based on field measurements (adjusted R^2: 0.14), proving it unsuitable for the part of the Romperöd forest characterized by selective thinning.

Keywords: Forest inventory, selective thinning forestry, boreo-nemoral forest, remote sensing, land cover classification, LiDAR, digital elevation model (DEM), canopy height model (CHM), above-ground biomass (AGB).

Sammanfattning

Att kvantifiera skogsinformation angående exempelvis marktäcke, terräng, trädhöjder och biomassa är en traditionellt både tidskrävande och dyr del av skogsbruk och skogsforskning eftersom mätningar vanligtvis samlas in i fält med handhållna instrument. Fjärranalys har visat sig vara ett värdefullt komplement till fältbaserade mätningar eftersom det möjliggör för snabb och relativt billig insamling av data från områden som skulle vara svåra att besöka i fält. Syftet med denna uppsats var att kartlägga och kvantifiera Romperödskogen utanför Glimåkra i nordöstra Skåne. Skogen har skötts genom blädningbruk sedan 1960-talet och omger en mast där mikrometeorologiska mätningar samlas in som en del av ett forskningsprojekt som avser att studera effekten olika skogsbruksmetoder har på växthusgasbalansen i skogar. Kvantifieringen genomfördes med hjälp av högupplösta multispektrala flygbilder och LiDAR-data inkluderad i den nationella höjdmodellen i kombination med mätdata som samlats in i fält. Resultaten blottlade en blandskog där gran utgör det dominerande trädslaget (40,2 % av den totala arean av studieområdet), följt av tall (13,8 %), lövträd (8,7 %), föryngringar (6,7 %) och bar mark (4,1 %). Den objektbaserade marktäckesklassificeringen resulterade i högre träffsäkerthet än den pixelbaserade metoden vilket demonstrerar vikten av segmentering och av att inkludera både spektral, texturell och rumslig information vid klassificering av högupplöst data över komplexa studieområden, som t.ex. en heterogen skog. Terrängen varierar från 76,2 till 107,3 meter över havet med en ås som sträcker sig från söder till norr. Höjden på krontaket är heterogent i hela studieområdet och varierar mellan 1,0 och 34,6 m med en medelhöjd på 15,1 m och en standardavikelse på 8 m. Biomassa ovan jord uppskattades med hjälp av LiDAR-data i kombination med fältmätningar och visar ett medelvärde på 122 900 kg/ha och en standardavikelse på 50 497 kg. Modellen förklarar 70 % av variabiliteten i de fältinmätta skattningarna. Resultaten jämfördes med biomassa ovan jord enligt SLUs Skogskarta som visade låg korrelation med skattningar baserat på fältmätningar (justerat R^2: 0,14) vilket visar att SLUs Skogskarta ej är applicerbar för den del av Romperödskogen som kännetecknas av blädning.

Nyckelord: Skogsinventering, blädningsskogsbruk, boreo-nemoral skog, fjärranalys, marktäckesklassificering, LiDAR, digital höjdmodell, trädkronhöjdmodell, biomassa ovanjord.

Table of contents

1. Introduction 1
2. Background 3
2.1 Forestry in Sweden 3
2.2 Forestry in Romperöd 5
2.3 Research station in Romperöd 6
2.4 Remote sensing in forest applications 7
3. Materials and Methods 11
3.1 Study area 11
3.2 Method overview 13
3.3 Field measurements 14
3.4 Remotely sensed data 16
3.5 Field plot biomass estimations 17
3.6 Land cover classification 19
3.7 Digital elevation modelling 24
3.8 Biomass modelling 25
4. Results & Discussion 29
4.1 Field plot measurements and reference AGB estimations 29
4.2 Land cover classification 30
4.3 Digital terrain model 33
4.4 Canopy height model 35
4.5 Biomass model 38
4.6 Biomass comparison 40
4.7 Further scope 43
5. Conclusions 45
Acknowledgements 46
References 47
Online resources 53
Appendix I 57
Appendix II 58
Appendix III 59

1. Introduction

Global atmospheric greenhouse gas (GHG) concentrations have increased to levels exceeding the natural variations during the last 800 000 years, as determined by analyzing air trapped in Antarctic ice cores (Lüthi et al, 2008). Annual global GHG emissions grew from approximately 28.7 to 49 Gigatons of carbon dioxide (CO_2) equivalents, or by 70 %, between 1970 and 2010 (IPCC, 2014). The main cause for the increase is emissions from fossil fuel combustion and industrial processes (about 78 %) but a significant part of it can be contributed to land use change, mainly deforestation, which accounted for about 11 % of the annual anthropogenic GHG emissions in 2010 (IPCC, 2014).

Forests play an important role in controlling the global climate system as vegetation consumes atmospheric CO_2 through photosynthesis and stores it as organic biomass in a process called sequestration (Pan, 2011). It has been estimated that intact forests and forest recovering after disturbances (e.g. after a harvest or after being wind thrown) globally sequestered around 4 billion tonnes of carbon annually between the years of 1990 and 2007, equivalent to almost 60 % of the CO_2 being released into the atmosphere from fossil fuel emissions during the same time period (Pan, 2011). The majority of the sequestered carbon the past two decades has been stored in the temperate and boreal forests across the globe (Reich, 2011).

When forests are burned or cut down, photosynthesis cease and the carbon stored in the trees is released into the atmosphere as the organic material decomposes. If the forest is converted to other land use types (e.g. agriculture) future possible sequestration is lost as well (IPCC, 2014). Deforestation and forest degradation due to agricultural expansion, conversion to pastureland, destructive logging, fires etc. are the second biggest source of CO_2 to the atmosphere (after the energy sector) and has been estimated to account for up to 20 % of the global greenhouse effect (UN-REDD, nd).

To study the effects different forestry practices have on the GHG balance of ecosystems, a tower was set up in 2013 in Romperöd, a forest in southern Sweden where selective thinning has been practiced for decades, to measure fluxes of CO_2 and H_2O. The research conducted there is part of the research project “Effect of forest management on climate forcing - accounting for all greenhouse gases and energy balance" funded by The Swedish Research Council Formas. The project aims to quantify GHG fluxes from different forest types to determine if they are sources (net release) or sinks (net uptake) of GHGs.

Traditionally, collecting forest information about e.g. land cover, tree height and estimates of volume has been a both time-consuming and labor-intensive part of forestry and forest research as field measurements typically are collected manually using handheld equipment (Kangas & Maltamo, 2006). Advantages of remote sensing include the ability to collect measurements with high speed and relatively low cost and the possibility to collect data in areas that are difficult to access on the ground (Gibbs et al, 2007). The aim of this thesis was to map and quantify the Romperöd forest using remote sensing data in conjunction with field measurements. The study can be broken up into three main objectives:

1. **Land cover mapping**
   - How are different land cover classes distributed in the forest? The hypothesis is that high resolution aerial images can be used to distinguish between the different tree species occurring at the Romperöd site.
2. **Characterization of the terrain and canopy cover**
   - Is the landscape hilly or flat? Is the canopy cover homogenous or heterogenous? The hypothesis is that the canopy cover in the Romperöd forest is vertically heterogeneous.
3. **Biomass modelling**
   - How large is the above-ground biomass (AGB) storage? The hypothesis is that the LiDAR data included in the national elevation model is detailed enough to be used to estimate AGB in the Romperöd forest.

Landcover and biomass mapping is important for forest management planning and can be used to monitor future changes or disturbances in the forest (Goetz et al, 2009). Accurate AGB estimates are important as AGB readily can be converted to carbon storage which is a vital step in understanding the carbon cycle of forest ecosystems (Malhi et al, 2002). Furthermore, knowledge about the terrain and vegetation surrounding the flux tower is important when interpreting the data and can be used for precise modelling of the spatial representativeness (footprint) of long-term accumulated eddy-covariance measurements (Gökede et al, 2006; Vesala et al, 2008).

2. Background

2.1 Forestry in Sweden

Out of Sweden's total 40.7 million ha land area, about 28 million ha (57 %) is covered by productive forest (Swedish Forest Agency, 2014). The carbon stored in forest biomass amounts to more than 1010 million tonnes (Mt) where stem wood biomass accounts for approximately 55 % while the rest is stored in the branches, needles, stumps and roots of the trees (Olsson, 2010). The yearly growth of the forests biomass is approximately 80 Mt, equaling 40 Mt of carbon, or an uptake of 145 Mt CO_2 (Olsson, 2010). A lot of this uptake is lost due to logging but since the harvest level has been well below the growth, the carbon storage increased by almost 8 Mt a year between 2000 and 2010 which equals an annual CO_2 uptake of 28 Mt (Swedish Environmental Protection Agency, 2015), or about 55 % of the CO_2 emissions produced in Sweden stemming from the burning of fossil fuel and production of cement during the same time period (The World Bank, 2015). The most dominating tree species is Norway spruce *(Picea abies)*, accounting for 42 % of the standing volume followed by Scots pine *(Pinus sylvestris)* (39 %) and silver and downy birch *(Betula pendula & Betula pubescens)* (12 %). The remaining 7 % is mainly constituted of broad-leaved species (The Swedish Forest Agency, 2014).

The vast majority of the Swedish forests are managed with some type of clear-cut forestry, an annual average of 189 600 ha of forest was clear-cut in the period between 2009 and 2013 (The Swedish Forest Agency, 2014). Clear-cut forestry in Sweden is typically characterized by homogenous coniferous forest stands in which all trees are planted at the same time (Albrektson et al, 2012). While the planted trees still are young, undergrowth cleaning and pre-commercial thinning is carried out to clear from naturally generated vegetation (which typically is left on top of the forest floor) to give additional space and nutrients to the production trees (Albrektson et al, 2012). Before the final felling, the forest is usually thinned at least two times, removing between 20 % and 40 % of the standing volume each time, to focus the production capacity of the forest on a smaller number of trees (Albrektson et al, 2012). When the remaining trees have reached a thickness of around 30 cm at breast height, clear-cutting is carried out. Allowing the trees to grow thicker increases the risk of rot and storm fellings and is therefore not economically justifiable (Södra, 2011). After the forest has been cleared, ground preparations are carried out to prepare for a new generation of planted saplings (Albrektson et al, 2012). The time it takes to complete this cycle (from saplings to

harvested trees) depends on the productivity of the forest but the forestry act §10 (Law 2008:662) regulates that spruce must be at least 45-90 years old before it can be cut down (depending on the location and productivity of the forest) while pine must be 60-90 years old.

Several carbon balance research projects around the world have shown that clear-cutting leads to drastic changes in the carbon dynamics of the ecosystem (Mäkiranta et al, 2010, Paul-Limoges et al, 2015). The main cause for these changes is a loss of photosynthesizing biomass and enhanced ecosystem respiration due to easily decomposable organic matter, i.e. dying tree roots and logging residue (Mäkiranta et al, 2010). An example from a study in Canada showed that a clearing transformed a mature fir forest, previously acting as a moderate sink (net ecosystem exchange (NEE) of -2053 g CO_2 m^{-2} yr^{-1}) to a major source of carbon to the atmosphere (NEE = 3667 g CO_2 m^{-2} yr^{-1}) (Paul-Limoges et al, 2015). A study on a pine peat forest in Finland showed similar results, with an average NEE of 1990 g CO_2 m^{-2} yr^{-1} the following three years after clear-cutting and concluded that even though the ground vegetation recovers fast after a clearing and starts to store carbon, the presence of a new forest stand is needed before the forest can act as a sink again (Mäkiranta et al, 2010).

Alternative forestry practices are still uncommon in Sweden even though forest owners have been free to use them since the new Forestry Act of 1993 when the old legislation, focusing on maintaining high yield and forcing the forest owners to practice clear cut forestry, were replaced by new laws, placing equal focus on production and nature conservation (Westerstad, 2011). Continuous cover forestry is a group of methods that has gained increased interest in the Nordic countries (Andersson, 2006). Selective thinning is an example of a continuous cover forestry practice characterized by uneven-aged forests which are selectively thinned with relatively frequent intervals, while leaving the majority of the trees untouched (Lundqvist et al, 2009). This encourages increased growth in the remaining trees as more sunlight and nutrients are made available (Lundqvist et al, 2009). The extracted trees are eventually replaced by new saplings through natural rejuvenation and there is therefore often no need for manual plantations (Oleskog, 2008). Selective thinning has many ecological benefits compared to clear-cut forestry as a continuous and unfragmented forest cover constitutes a necessary habitat for many forest-living species. According to the Swedish Red List, 861 forest-living species are considered as threatened and 270 as near-threatened (The Swedish Forest Agency, 2014). A recent study, comparing the biodiversity of natural forests with forests where clear-cut forestry and forests where selective thinning is being practiced

showed that clear-cut forests have significantly lower species diversity compared to selectively thinned forests where the biodiversity was similar to natural forests (Leverin, 2014).

2.2 Forestry in Romperöd

The Romperöd forest has a long tradition of selective thinning (D. Göransson, personal communication, April 14th, 2015; Göransson, 2015). Around 1920 all coniferous trees that had reached a profitable dimension were cut to finance a generation shift at the farm, leaving a residual forest with broadleaved trees of varying size and coniferous trees not thicker than 12 cm at breast height. During the 1940s, some deciduous trees were felled for firewood. This resulted in an uneven-aged forest, which prompted the forest owners to carry out selective thinning in 1946 and 1959 with the purpose of evening out the canopy layer. The effect however, was the opposite. Sometime during the 1960s, the owners decided to fully commit to selective thinning and started to develop the silviculture which is carried out today (D. Göransson, personal communication, April 14th, 2015).

Out of Romperöd's approximately 120 ha forest, about 40-60 ha is currently characterized by selective thinning which is carried out according to the following summarized principles (a complete list can be found in Appendix I) (D. Göransson, personal communication, April 14th, 2015):

- Cut primarily the biggest trees – spruce should not reach a diameter (at breast height), that exceeds 60 cm (maximum for debarking machinery). Normally this means that spruces bigger than 50 cm should not be left.
- Slow growing trees and trees with low timber quality in the upper canopy story should be cut to promote quality and height on the remaining trees and to forward good genes to new generations of saplings.
- The production should be focused on big and valuable trees while it is less important to increase the growth of smaller trees by thinning dense groups of trees. The high tree density will improve timber quality.
- Trees smaller than the smallest profitable dimensions should normally only be cut if the quality of the trees are so bad that they will not grow into sellable timber.
- Do not thin more than 35 % of the standing volume to prevent storm damage. Leave wind resistant trees, especially pine, and avoid opening pathways for westerly winds.

- Keep a standing volume high enough (at least 100 m3/ha, preferably 150 m3/ha or more) to uphold high production and to facilitate natural rejuvenation.
- Try to always keep the forest floor shadowed. This is especially important for stands on dry ground. Shadows prevent wavy hair grass *(Deschampsia flexuosa)* and broadleaved trees from establishing and promotes rejuvenation of shadow tolerant tree species like Norway spruce *(Picea abies)* and Scots pine *(Pinus sylvestris)*.

2.3 Research station in Romperöd

In June 2013 a research team from Lund University started a measurement station in the Romperöd forest, with the main purpose of quantifying net CO_2 fluxes to determine the carbon balance of the forest and in that way study the effects selective thinning forestry has on the climate. A 35 m high tower (Figure 1) was erected to conduct micrometeorological measurements of CO_2 and H_2O fluxes using an ultrasonic anemometer and an infrared gas analyzer and utilizing the eddy covariance technique (Burba, 2013). In addition to this, other parameters measured include energy fluxes, relative humidity, air temperature, precipitation, soil temperature, soil moisture, and soil conductivity.

Figure 1. The Romperöd flux tower during maintenance.

2.4 Remote sensing in forest applications

Remote sensing is a powerful tool that has been widely used over the last decades to map and model forest ecosystems (Lavrov et al, 2003; Chu, 2014). Passive remote sensing sensors (e.g. aerial photography) measure naturally available electromagnetic radiation (reflected sunlight) in different wavelength bands or absorbed and re-emitted thermal energy (Lillesand et al, 2008). Active sensors (e.g. RADAR) on the other hand, transmit their own source of illumination and measure the amount of energy being reflected back to the sensor (Lillesand et al, 2008). A combination of both passive and active sensors is commonly used in forest applications, for example, Ranson et al (2003) fused multispectral images from the Landsat-7 satellite system with RADAR data from a range of satellite systems to map burned areas, logging, and insect damage in the boreal forests of Siberia and Holmgren et al (2008) used multispectral aerial images in combination with high resolution LiDAR data for species identification of individual trees in a temperate mixed forest in southern Sweden. Other forest applications related to remote sensing include e.g. forest management planning, land cover type discrimination, habitat mapping, forest health assessments and monitoring of forest recovery after storm fellings or wildfires (Lavrov et al, 2003; Hyde et al, 2006; Chu, 2014; de Tanago et al, 2014).

2.4.1 Land cover classification

Different materials on Earth reflect and absorb incident sunlight in different parts of the electromagnetic spectrum. Vegetation reflects mostly in the near infrared (NIR) and green parts of the spectrum as can be seen in Figure 2. Green leaves reflect about 20 % of the sunlight in the green to red wavelength bands (0.5-0.7 μm) and about 60 % in the NIR band (0.7-1.3 μm) (Loveland et al, 1991). The spectral profile of bare ground depends on material but generally shows higher reflectance in all bands. Shadows have the lowest reflectance in all bands as no direct sunlight is reflected from the surface. These spectral differences make it possible to identify and map objects and materials in remotely sensed images using automated classification algorithms (Lillesand et al, 2008).

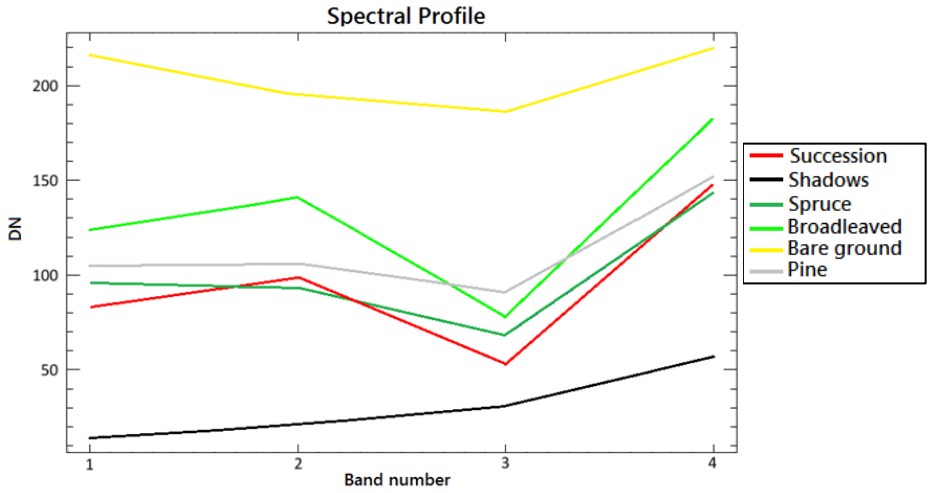

Figure 2. Spectral profile of the classes chosen for the land cover classification based on the data from 2010 described in section 3.4. 1 = blue, 2 = green, 3 = red and 4 = near-infrared, DN = digital number*

* Digital number (DN) is commonly used to describe pixel values that have not yet been calibrated into physically meaningful units.

An example of a widely used classification algorithm is the Support Vector Machine (SVM) (Boser, Guyan, and Vapnik, 1992). SVMs are a group of machine learning methods that have proved to be especially good at classifying noisy or complex data (Melgani and Bruzzone, 2004; Pal and Mather, 2005; Lu and Weng, 2007). Given a set of training examples, SVMs classify data by computing an optimal hyperplane in linearly separable patterns (Boser, Guyan, and Vapnik, 1992). The training examples are projected as points in two-dimensional space and separated by a straight line. The predicted class values are decided depending on which side of the line a pixel or feature is mapped. Since complex data cannot always be separated by straight lines in two-dimensional space, a non-linear kernel function is often applied, projecting the inputs into high-dimensional feature space where an optimal hyperplane can be computed to separate them into classes (Boser, Guyan, and Vapnik, 1992).

Traditional remote sensing classification techniques are pixel-based which means that an image is classified based on individual pixel values representing reflected electromagnetic radiation (Lillesand et al, 2008). Pixel-based classification methods work well with hyperspectral data but are not ideal when it comes to classifying high resolution multispectral imagery (Blaschke, 2003). A more modern approach is to use an object-based classification method. In object-based methods the pixels of an image is first grouped into features, or objects, typically sharing spatial, spectral, and textural properties (Nielsen, 2014). The

classification is then based on these objects rather than the individual pixels. Object-based classification is particularly suitable for medium to high resolution data as objects in the image, like trees or buildings often consist of several pixels with varying spectral properties (Clark Lab, 2009).

2.4.2 Estimating biomass

Estimating biomass via field measured forest inventory data is both time-consuming and expensive and is therefore generally only repeated at ten-year intervals (Houghton, 2005). The possibility of estimating biomass using remote sensing is therefore considered to be a valuable alternative, or complement, to field-based forest inventories (Hese et al, 2005).

Remote sensing estimates of AGB is often conducted using a combination of field measurements and both active and passive remote sensing systems (Goetz et al, 2009; Pirotti, 2011; Shendryk, 2013; Cao, 2014). However, it is still a challenging task in terms of model complexity and data availability (Shendryk, 2013). Active systems like e.g. the synthetic aperture radar (SAR) have been used to model AGB with satisfying results (Robinson et al 2013). SAR measures the height of objects by sending radio pulses on the Earth surface and records the backscatter of the reflected pulse, however, the sensitivity and accuracy of such instruments have shown to decrease with increasing AGB due to a saturation effect on the backscatter occurring at high AGB values as the canopy cover gets too thick and opaque for the radio pulse to penetrate (Mitchard et al, 2012; Robinson et al, 2013). Passive systems, like multi- and hyper-spectral optical sensors, are capable of mapping some aspects of forest structure but have difficulties penetrating beyond the upper canopy layer and are therefore more suited for mapping horizontal components, like land cover type (Weishampel et al, 2000). LiDAR sensors have proved to be a promising alternative to conventional sensors for modelling AGB thanks to the high intensity and frequency of the pulses being emitted from the instrument which makes it capable of penetrating even a thick canopy cover and makes it suitable for smaller-scale studies (Hyde et al, 2007).

2.4.3 LiDAR Analysis

LiDAR stands for light detection and ranging and was developed more than 20 years ago as a tool for terrain mapping (Baltsavias, 1999). It is an often airborne active remote sensing technology that sends high frequency laser pulses at the Earth’s surface and measures the time delay between the transmission of the pulse and the detection of the reflected signal to

determine the elevation of the terrain and the height of objects occupying it (Lefsky et al, 1999). Compared to RADAR technology, which utilizes radio waves, LiDAR uses much shorter wavelengths, typically in the ultraviolet, visible or near-infrared range of the electromagnetic spectrum (Lavrov et al, 2003).

There are two types of LIDAR systems, differentiated by how the backscattered laser pulses is quantified and recorded by the system's receiver. Full-waveform LiDAR systems records the entire waveform of each pulse reflected back to the sensor at fixed time intervals (typically ~1 ns) (Pirotti, 2011). In contrast, small footprint discrete-return LiDAR systems normally records several returns for the same pulse, the first return from the uppermost part of the canopy, followed by less intense returns through the canopy down to the forest floor (Lavrov et al, 2003). Both types of LiDAR systems are utilized in forest applications to measure the three-dimensional structural characteristics of a forest and its underlying terrain (Van Leeuwen and Nieuwenhuis, 2010; Cao, 2014; de Tanago et al, 2014). These characteristics are often used to model e.g. forest volume, basal area and productivity (Nilsson, 1996; Nelson et al, 1997; Lefsky et al, 1999). LiDAR can also be used for habitat mapping and forest wildlife management as the presence of specific organisms, bird species and the overall richness of wildlife communities can be highly dependent on the structural patterns of the forest (MacArthur and MacArthur, 1961; Carey et al, 1991).

A digital elevation model (DEM) is a 3D representation of a terrain's surface and is a common product to derive from LiDAR data (Augilar et al, 2010). DEM is often used as a collective term for both digital terrain models (DTM), digital surface models (DSM) and canopy height models (CHM). A DTM, or bare-earth image, represents the Earth's surface without any objects on it and can be computed using the ground returns of small-footprint LiDAR data (Schwarz, 2012). In contrast a DSM depicts all the objects on the Earth's surface, like trees or houses and is generated using the first LiDAR returns (Schwarz, 2012). A CHM represents the height of the forest canopy above ground level and is produced by subtracting the DSM from the DTM (Schwarz, 2012).

Studies have shown that LiDAR derived CHMs have great potential when it comes to estimating the AGB of a forest (Couteron et al, 2012; Cao, 2014). Ideally, CHMs are divided into individual tree crowns using segmentation algorithms (Shendryk, 2013). Species specific allometric AGB functions, derrived using field measured tree heights as predictor variable and

field measured AGB estimates as response variable, are then typically applied to all separable trees in the CHM individually (Cao, 2014).

3. Materials and Methods

3.1 Study area

The Romperöd forest is located outside Glimåkra in north-eastern Scania, Sweden (56° 20’00” N 14° 06’45” E) (Figure 3). The study area covers the part of Romperöd characterized by selective thinning (approximately 52.5 ha).

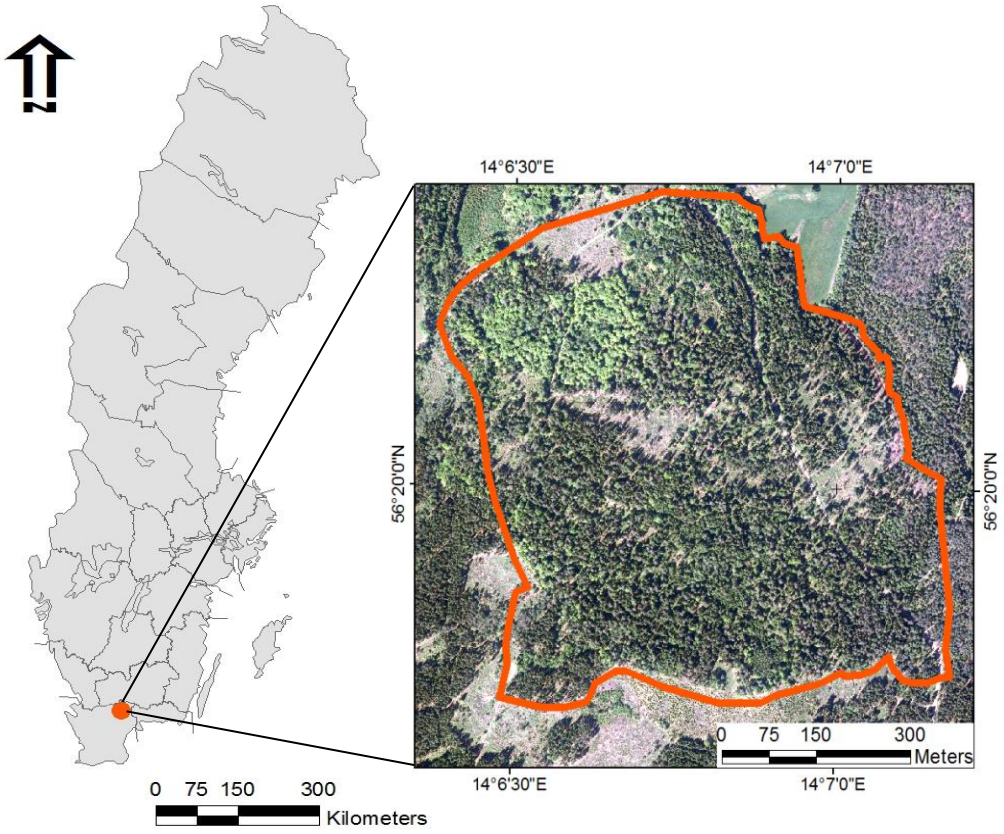

Figure 3. The red dot pinpoints the location of the Romperöd forest in north-eastern Scania, Sweden. The red border in the aerial image outlines the study area. © Kommunerna i Skåne

The most dominating soil type in the area is sandy moraine but fen peat can also be found (SGU, 2015). The silviculture practiced has led to a highly diverse forest, both regarding species and age-class distribution (D. Göransson, personal communication, April 14th, 2015). The most dominating tree species is Norway spruce *(Picea abies)*, but Scots pine *(Pinus sylvestris)*, English oak *(Quercus robur)*, European beech *(Fagus sylvatica)*, silver birch *(Betula pendula)* and downy birch *(Betula pubescens)* are also common (D. Göransson,

personal communication, April 14th, 2015). The forest floor is covered with bilberry *(Vaccinium myrtillus)*, mosses, and lichens and signal species indicating high nature values can be found (Leverin, 2014). Examples, showing the variation of the Romperöd forest can be seen in figure 4 a-f.

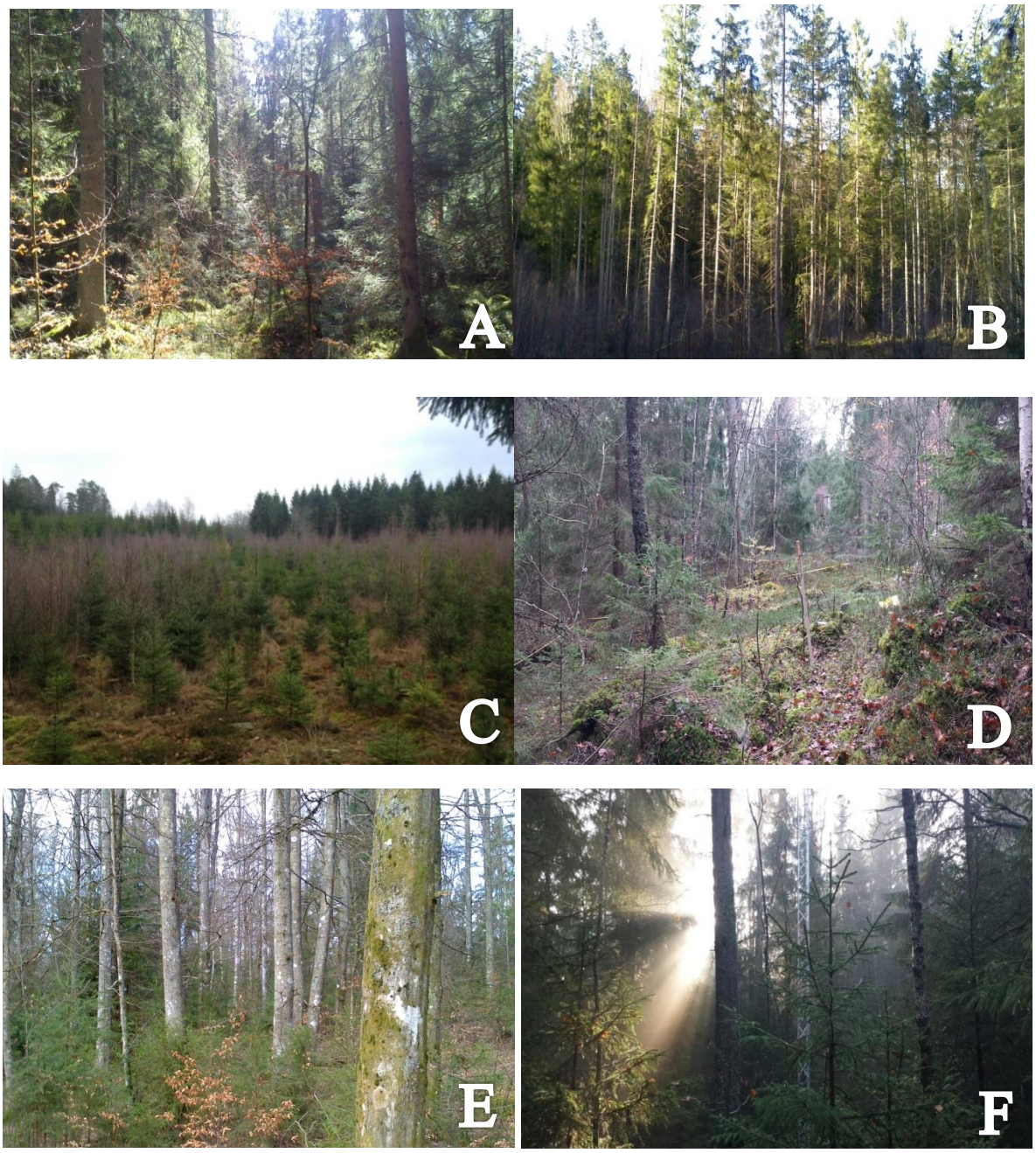

Figure 4. A) Typical mixed forest in Romperöd. B) Spruce forest stand. C) Wind thrown area with natural plant succession taking place, resulting in a mix of spruce and pine saplings together with taller birch. D) Young mixed forest E) Beech forest with some small spruce trees around. F) Vegetation around the research tower (the base of the tower can be seen in the center of the picture).

3.2 Method overview

The characterization of the Romperöd forest was carried out using several different methods, equipment, and software and can be broken up into five parts:

- **Field measurements** – where information about tree species, measures of tree trunk diameter at breast height (DBH) and tree heights were manually collected in field plots.
- **Reference biomass estimations** – AGB was estimated for the field plots using the forest variables mentioned above and empirical biomass functions.
- **Land cover mapping** – Both a pixel-based and an object-based land cover classification were carried out on high resolution multispectral aerial photography and compared using ground truth points collected in field.
- **Digital elevation modelling** – where a DTM and a CHM were extracted from LiDAR data to characterize the vertical structure of the forest and its underlying terrain. Accuracy assessment was conducted using ground elevation and tree heights measured in field.
- **Biomass estimates for the whole study area** – The AGB estimates based on the field plot measurements were upscaled to cover the entire study area. AGB was also estimated using LiDAR metrics as predictors in a regression model. Finally, the results were compared with estimates from other sources.

3.3 Field measurements

Forest parameters (tree species, tree height and DBH) were measured for 18 field plots (Figure 5) to be used to estimate reference biomass, serve as input for the regression analysis carried out and to assess the accuracy of the results.

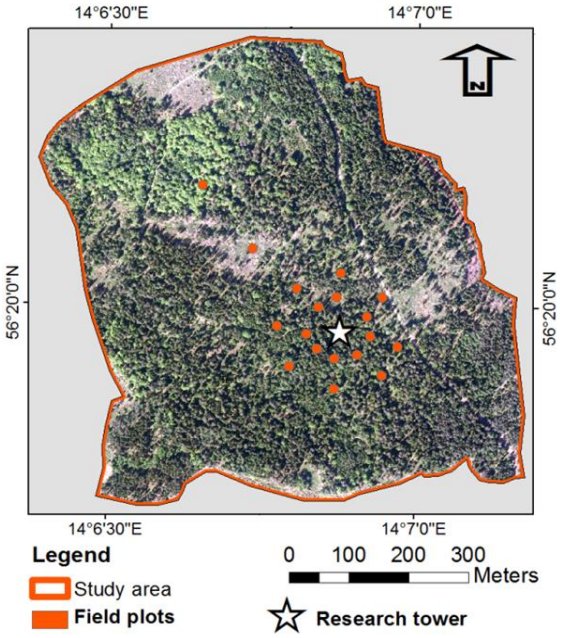

Figure 5. Aerial view of the study area with the field plots marked by red dots and the flux tower by a white star.

Eight field plots were already measured in the summer of 2014 and data were provided by the Department of Physical Geography and Ecosystem Science at Lund University. Ten new field plots were sampled between November 15th, 2014 and March 10th, 2015. The locations of the plots were chosen in the same way as the previous ones, by systematic sampling in four different cardinal directions around the flux tower (white star in figure 4). As the old sites were located 50 and 100 m away from the tower in northern, eastern, southern and western directions, four new cardinal directions with the same distance to the tower were used for the new sites (NE, NW, SE, SW). Two additional plots were chosen in the NW direction to include a young birch forest in a wind thrown opening 200 m from the tower and a mature beech forest 325 m from the tower.

All field plots were circular with an area of 200 m^2. The extent of the field plots was defined using a Vertex IV hypsometer (Haglöf Sweden AB; Haglöf, 2012). The hypsometer uses ultrasonic signals to measure the distance between the instrument and a transponder placed in the center of each field plot. The height of the trees within each field plot was measured by fastening the transponder on a tree trunk at breast height (130 cm). The instrument was then aimed at the transponder and then at the top of the tree crown where several readings were saved (Figure 6). The height of the tree is calculated based on the average distance and angle between the instrument and the transponder and the angle between the instrument and the top of the tree. The hypsometer has a horizontal resolution of 0.01 m and a vertical resolution of 0.1 m according to the manual (Haglöf, 2012).

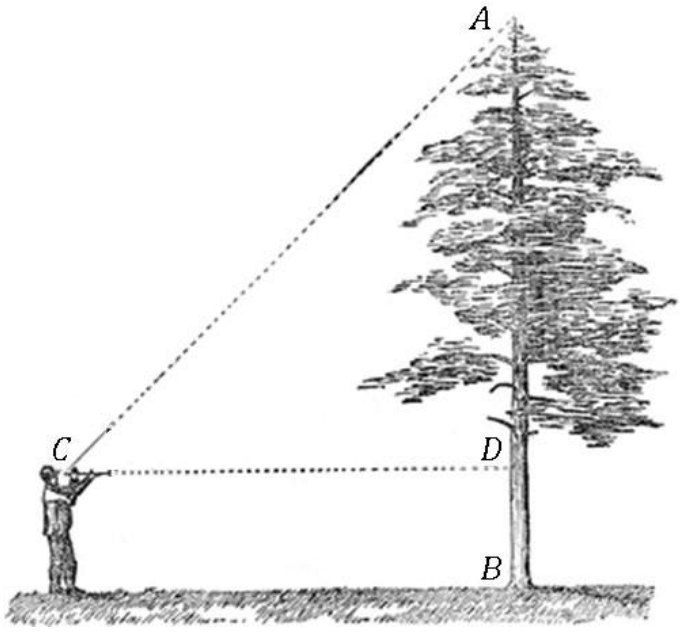

Figure 6. The vertex measuring procedure where A is the top of the tree, B is the ground level, C is the instrument position and D is the transponder position (from Haglöf, 2012).

The DBH of all trees was measured two times in opposite directions around the tree trunk and averaged to get one representative DBH for each tree. Only trees higher than 2 m and with a DBH above 3 cm were measured as the allometric functions used to estimate AGB (described in section 3.6) do not apply for smaller trees and because the biomass of these trees was considered insignificant in relation to the total AGB.

Center coordinates, including elevation above sea level, were collected for all field plots using a Topcon GRS-1 global navigation satellite system (GNSS) receiver together with an external antenna (PG-A1) (Figure 7). The GRS-1 uses signals from both GPS and GLONASS satellites to reach an accuracy of one meter or better. The external antenna enables real time kinematic (RTK) data collection on a centimeter level by receiving correction signals from the Swedish Land Survey via a GSM cellular modem (Topcon, 2009). The horizontal accuracy while measuring the field plots pended between 1 and 30 cm and the vertical accuracy was approximately 1 m according to the instrument.

Figure 7. The Topcon GRS-1 and the external antenna attached to a 2 m carbon pole.

Ground truth data for assessing the accuracy of the image classification were collected by visiting 150 points in field using the Topcon GRS-1. A point generator was used to randomly distribute two points within each cell of a 10x10 grid system covering the study area (ESRI, 2014). The minimum allowed distance between points was restricted to 20 m to spread the validation points evenly over the study area and to avoid local clusters of points in the same land cover class. For each visited point, the land cover was recorded. If a point was in an unsuitable location, like in a swamp or between different land cover classes it was moved to the closest appropriate spot where the land cover was possible to determine. All coordinates were stored as a point file in SWEREF99 TM, the Swedish national geodetic reference system. Ten of the points were later discarded after plotting them above the aerial image as adjacent canopies made it hard to delineate their land cover class, leaving 140 points remaining. The horizontal accuracy while locating the points in field pended between 1 and 50 cm according to the instrument.

3.4 Remotely sensed data

3.4.1 Spectral data

Two aerial multi-spectral photos were used for the land cover classification. The images were made available through collaboration between Geodatacenter Skåne AB and the GIS centre at Lund University. Both images were collected on June 2nd, 2010 using a large format digital aerial camera (Vexcel UltraCamXp) mounted on an aircraft flying at an altitude of 2900 m (Strandberg, 2010). The images consist of four spectral wavelength bands (red, green, blue and near-infrared) and have a spatial resolution of 25 cm (Strandberg, 2010).

To correct for radial displacement the data had been orthorectified (adjusted for topographic relief, lens distortion and sensor tilt). The resulting orthophoto is an accurate representation of the Earth's surface, which allows for direct measurements of distances, angles and areas. To achieve this, aerial triangulation techniques has been carried out using measured ground elevation points together with elevation data from the new national elevation model, resulting in an average horizontal deviation of 0.06 m and an average vertical deviation of 0.30 m (Strandberg, 2010).

Two additional aerial orthophotos from May, 3rd, 2012 were acquired to be used for shadow filling. The imagery was gathered and processed by the Swedish Land Survey using a digital mapping camera (Z/l DMC01-0050) mounted on an aircraft flying at 2500 m altitude (The Swedish Land Survey, 2012). The images were made available by the Swedish University of

Agricultural Sciences through their geographic extraction tool (GET). The images have been collected in three wave length bands (red, green and blue) and have a spatial resolution of 1 m.

All spectral data were referenced according to the Swedish national geodetic projected coordinate system SWEREF 99 TM.

3.4.2 LiDAR data

A discrete-return small-footprint LiDAR dataset was acquired from GET. It was collected between April 2nd and April 3rd, 2010 using a Leica ALS50-II LiDAR system mounted on an aircraft flying at an altitude of 1700-2300 m with a scanning angle of ± 20° and a footprint size of 0.5-0.7 m (The Swedish Land Survey, 2011). The dataset includes two point clouds covering the study area with an average point density of 0.85 points/m^2. The data has been referenced to the SWEREF 99 TM projected coordinate system and RH2000 height system. The vertical mean accuracy is 0.1 m and the horizontal mean accuracy is 0.3 m, assessed using field measured validation points (The Swedish Land Survey, 2011).

3.4.3 Reference AGB data

A biomass raster layer was acquired from the SLU Forest Map (earlier known as kNN-Sweden), freely available from the Swedish University of Agricultural Sciences (SLU). The biomass estimation is based on satellite data from 2010 (same year as the main spectral image and the LiDAR data) provided by the national land survey in their geoportal SACCESS and the National Forest Inventory (SLU, 2015). The layer has been referenced in RT90 2,5 gon V and has a spatial resolution of 25 x 25 m.

3.5 Field plot biomass estimations

Aboveground biomass (AGB) will in this study refer to the total dry biomass of the stem and bark (ST) and the branches and foliage (CR) of the tree and was estimated for all tree types within the field plots using empirical functions (Table 1). AGB was used instead of carbon content to be able to compare the results with AGB estimations from other sources. The relationship between the biomass and carbon content of vegetation typically varies between 45 and 50 % (Schlesinger 1991). A study from Ireland, comparing five even-aged monospecies Sitka spruce (Picea sitchensis) stands ranging from 9 to 45 years old found that the carbon content of the mean tree component varied between 45.1±0.48 % to 46.5±0.84 % and that the ratio showed no significant difference with age and size of the tree (Tobin and

Nieuwenhuis, 2007). This shows that AGB can with fairly high accuracy be directly converted to carbon storage.

Table 1. Summary of the functions used for biomass estimations. H = tree height (m), DBH = diameter at breast height (cm), n = number of trees used for deriving the function, R^2 = coefficient of determination, a-d = model parameters, ln = natural logarithm, CR = crown biomass (kg), ST = stem biomass (kg) and AGB = aboveground biomass (kg). The functions have been derived by empirical studies of the relationship between DBH, tree height and AGB (Marklund, 1988; Johansson, 1999; Hochbichler, 2002; Brandini & Tabbachi, 1996).

Tree species	Output	n	R^2	Equation	a	b	c	d
Spruce	ln(CR)	544	0.95	$a+b\cdot[DBH/(DBH+13)]+c\cdot H+d\cdot \ln(H)$	-1.2063	10.9708	-0.0124	-0.4923
Spruce	ln(ST)	546	0.99	$a+b\cdot[DBH/(DBH+14)]+c\cdot H+d\cdot \ln(H)$	-2.1702	7.469	0.0289	0.6858
Pine	ln(CR)	482	0.92	$a+b\cdot[DBH/(DBH+10)]+c\cdot \ln(H)$	-2.5413	13.3955	-1.1955	-
Pine	ln(ST)	488	0.99	$a+b\cdot[DBH/(DBH+13)]+c\cdot H+d\cdot \ln(H)$	-2.6768	7.5939	0.0151	0.8799
Oak	AGB	94	0.95	$a+b\cdot DBH^2\cdot H$	-0.6165	0.03582	-	-
Beech	ln(AGB)	42	0.99	$a+b\cdot \ln(DBH)+c\cdot \ln(H)$	-2.872	2.095	0.678	-
Birch	AGB	-	0.99	$a\cdot(DBH\cdot 10)^b$	0.00087	2.28639	-	-

Biomass fractions (ST and CR) were estimated for Norway spruce *(Picea abies)* and Scots pine *(Pinus sylvestris)* using functions developed by Marklund (1988) (Table 1). The Marklund functions describe the relationship between tree height, DBH and biomass fractions and have been derived by destructive sampling of 1286 trees in 131 different forest stands in Sweden after which the dry weight biomass has been measured. Both silver birch *(Betula pendula)* and downy birch (*Betula pubescens*) were estimated using a function for silver birch created by Johansson (1999). The function used yields AGB directly based on DBH and the two model parameters shown in Table 1. European beech *(Fagus sylvatica)* AGB was estimated using a function from a study conducted in Austria (Hochbichler, 2002). No appropriate function for English oak *(Quercus robur)* could be found so a function derived in an Italian study of Holm oak *(Quercus ilex)* was used in its place (Brandini & Tabbachi, 1996). Rowan *(Sorbus aucuparia)* and Alder *(Alnus glutinosa)* were also present in the field plots but very few and were therefore treated as birch and beech respectively. Using these functions instead of functions intended for the tree species might give rise to small estimation errors but these were considered insignificant in relation to the total AGB of the plots.

The AGB of the field plots was averaged and scaled to the entire study area to compare the results with the modelled AGB.

3.6 Land cover classification

Exelis Visual Information Solutions (ENVI) was used to carry out both a pixel-based and an object-based land cover classification approach (Exelis VIS, 2015).

3.6.1 Pre-processing spectral data

A normalized difference vegetation index (NDVI) was derived using the red and NIR wavelength bands. NDVI is a vegetation index used to quantify the concentration of green leaf vegetation which has proved to be highly correlated with biomass accumulation, leaf chlorophyll levels, leaf area index and the photosynthetically active radiation absorbed by a plant (Lillesand et al, 2008). NDVI is based on an inversed relationship between the reflection of healthy vegetation in the NIR and red bands and can be expressed as:

$$NDVI = \frac{(NIR-red)}{(NIR+red)} \quad (1)$$

where NIR is the near infrared wavelength band (700-1300 nm) and red is the red visible band (620–700 nm) (Lillesand et al, 2008).

NDVI values ranges from -1 to +1 and healthy vegetation is displayed with high values since the pigments in plant leaves (chlorophyll) strongly absorbs incident radiation in the red wavelength band for use in photosynthesis while the cell structure of the leaves strongly reflects NIR radiation (Lillesand et al, 2008). Rock and bare soil reflect highly in both bands and therefore yield index values close to zero while clouds, water and snow reflect more in the visible spectrum than in the NIR and therefore are represented with negative values (Lillesand et al, 2008).

NDVI was for this study calculated using digital numbers (DN) rather than actual surface reflectance and will therefore henceforth be referred to as pseudo NDVI (pNDVI). A true NDVI would need to be derived using surface reflectance, which is the fraction of the total incident solar radiant energy *(J)* reflected back to the sensor and has to be calibrated taking atmospheric effects (i.e. absorption from clouds and other atmospheric components) into account (Lillesand et al, 2008).

The images including the color (RGB) and near-infrared (NIR) bands were fused with the pNDVI layers to create five band composites. These composites were merged to create a

single mosaic covering the whole study area. A vector mask outlining the study area was then created and used to spatially subset the mosaics. This to ensure that only forest characterized by selective thinning was chosen and analyzed.

A stretch renderer was applied to the composites to increase the contrast in the images and to make it easier to distinguish between different land cover types when creating the training sites for the SVM classifier. A linear stretch of 2 % was chosen after visually comparing different alternatives. The stretch was achieved by computing a cumulative histogram and setting the lowest and highest 2 % of the values to 0 and 255 respectively after which all the intermediate values were linearly stretched.

3.6.2 Segmentation

The multiband mosaics were first reduced to single band images using a Sobel edge detection method (Jin, 2012). The procedure identifies features with distinct boundaries in the image (like trees or buildings) by finding the maximum gradient across all bands in the image. The output is an image where areas with high pixel contrast are represented by high gradient values and areas with uniform pixel values by low gradient values. To control how many segments that was created a cumulative distribution function was used to discard the lowest 25 % of the gradient values. The number was decided after visually previewing the segmentation result and comparing it to the unsegmented images through a movable magnification window on top of the images.

The Vincent and Soille watershed algorithm (Roerdink and Meijster, 2001) was applied but instead of using elevation data, the gradient images were used. The algorithm floods the image, starting from the lowest areas (gradient values) and partition it into basins (features with similar gradient values) based on where water coming from different basins would meet. The process stops when the theoretical water level has reached its highest peak in the landscape. The result is an image divided into segments separated by borders where each segment has been given the mean spectral values of the pixels within that segment.

A full-lambda schedule method (Robinsson, 2002) was used to aggregate small segments within large objects with rough texture (like canopies) where over-segmentation was a problem. The algorithm merges adjacent segments based on both spectral and spatial information and can be described mathematically as:

$$t_{i,j} = \frac{|O_i|*|O_j|}{|O_i|+|O_j|} * \left\|u_i - u_j\right\|^2 / length(\partial(O_i, O_j)) \qquad (2)$$

Where $t_{i,j}$ is the merging cost, $|O_i|$ and $|O_j|$ the area of two adjacent segments, $\|u_i - u_j\|$ is the Euclidian distance between the mean spectral values of the O_i and O_j segments and length($\partial(O_i,O_j)$) is the length of the common boundary shared by O_i and O_j.

The decision to merge O_i and O_j occurs when the merging cost ($t_{i,j}$) is less than a predefined threshold value (λ) (Robinson, 2002). The threshold was set to only merge the segments with the 15 % lowest λ values, to only merge spectrally similar segments.

3.6.3 SVM classification

Training sites were created for all major land cover types in the study area, the classes chosen were: spruce, pine, beech, oak, succession, bare ground, and shadows. The training sites for the shadow class were selected by applying a threshold to the digital numbers (DN) of the red wavelength band in the images. Histogram thresholding methods assume a bimodal distribution of values with shadows occupying the lower end of the histogram; in this case the threshold value was set to 60 to capture all shaded areas (Figure 8).

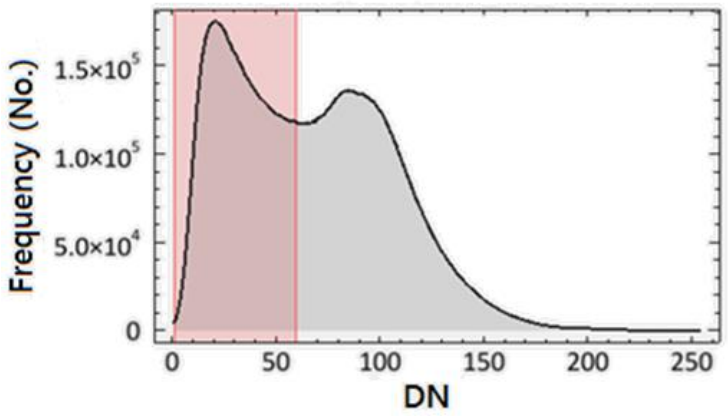

Figure 8. Distribution of digital numbers in the red wavelength band within the study area with shadows occupying the left side (0-60) of the histogram.

The other seven training classes were chosen by highlighting areas in the images and assigning class values to them based on the coordinates collected in field. A general recommendation is to create training sites with at least 10 to 100 times more pixels than the number of spectral bands of the imagery (Muise, 2011). Each training class therefore consisted of about 500 pixels as the images are composed of three and five spectral bands. Both the Jeffries-Matusita and the Transformed Divergence measures were computed to make sure that the training classes were spectrally separable (Richards & Richards, 1999).

A set of attributes, to be used in the classification, was computed for the images. The attributes can be grouped into spectral (e.g. brightness and color of the pixels), textural (e.g.

mean and variance), and spatial (e.g. area and shape) attributes (a complete list and description can be found in Appendinx II). The spectral attributes were computed on each of the five bands in the input image and were assigned to pixel-clusters sharing the same segmentation label. Texture attributes were computed in two steps. In the first step, a moving window with the size of 3x3 pixels visited each pixel in all bands of the input image. Attributes were then calculated for all pixels inside the window and referenced to the pixel in the center of the window. In the next step, the textural attributes were averaged across each pixel within the segments and assigned to that band's segmentation label. A small window size was chosen due to the heterogeneity of the forest and to enable classification of small areas with high texture variance, such as different tree canopies. The spatial attributes were computed using the polygons defining the boundary of the segments. Since the number of attributes computed was large, an interval based ranking technique was used to decide what attributes contributed the most to the classification. The algorithm ranks the significance of each attribute based on their ability to differentiate between classes provided in the training samples (Exelis VIS, 2007).

A Support Vector Machine (SVM) algorithm was applied to classify the rasters (Boser, Guyan, and Vapnik, 1992). The Gaussian radial basis kernel function was used as it often yields good results in SVM classifications and because the feature space of the kernel has an infinite number of dimensions (Chang et al, 2010; Amnon, 2009). The gamma parameter is the free parameter of the radial basis kernel function and was set to the reciprocal of the number of bands in the image (0.2) according to recommendations from Exelis VIS (2014). Mislabeled or unusual values in the training samples can give rise to a poorly fitted model. To account for this a penalty parameter was used. The parameter controls how big the effects of misclassifying training sites are by creating a soft margin that permits some training points on the wrong side of the hyperplane (Cortes and Vapnik, 1995). It was set to 100 which is a default value (Hsu, Chang and Lin, 2010). A lower penalty allow for a higher degree of misclassification of training samples while a higher value forces the creation of a more accurate model that may not generalize well.

3.6.4 Post-classification

To reduce the effects of shadows in the resulting land cover classification, the shadow class in the classified image from 2010 was replaced by the classes from the classified image from 2012.

A majority filter was applied to the pixel-based classification to eliminate isolated pixels and produce a more homogeneous landscape. This was done by applying a moving window with a size of 9x9 pixels to the classified image and replacing the central pixel with the most predominant class value.

3.6.5 Accuracy assessment

The results were evaluated and compared to determine the most accurate classification. Statistical accuracy assessment was conducted by comparing the 140 points collected in field with the corresponding land cover class mapped in the image and confusion matrices were computed. The confusion matrix compare, on a class-by-class basis, the relationship between the ground truth data and the output from the classification and was used to derive estimates of overall accuracy, class specific producer's and user's accuracy as well as the Cohen's Kappa statistic (Cohen, 1960).

The overall accuracy (Equation 3) gives the probability that a randomly chosen point (from field or map) is correctly mapped and is obtained by dividing the total number of correctly mapped pixels with the total number of reference points:

$$Overall\ accuracy = \frac{\sum A}{N} \qquad (3)$$

where sum of *A* is the number of correctly mapped points for all classes and *N* is the total number of points.

The producer accuracy (Equation 4) is a measure of omission and relates to the probability that a ground truth point will be mapped to the correct land cover class:

$$Producer's\ accuracy = \frac{A}{B} \qquad (4)$$

where *A* is the number of correctly mapped points in each class and *B* is the total number of ground truth points.

The user's accuracy (Equation 5) measures the level of commission and shows the probability that a sample from the land cover map matches the actual land cover from the ground truth points:

$$User's\ accuracy = \frac{A}{C} \qquad (5)$$

where *A* is the number of correctly mapped points in each class and *C* denote the total number of map data points.

The Cohen's Kappa coefficient (κ) (Equation 6) is an accuracy measure considered to be more robust than percent agreement calculations as it takes the agreement occurring by chance into consideration and can be described as:

$$\kappa = \frac{Nd - q}{N^2 - q} \qquad (6)$$

where *N* is the total number of points, *d* the sum of the correctly mapped points and *q* the sum of the products between the number of ground truth points and the number of map data points in each class. κ ranges from 0, when there is no agreement other than what would be expected by chance, to 1 when there is perfect agreement (Foody, 2002).

3.7 Digital elevation modelling

3.7.1 Terrain and canopy height modelling

The LiDAR dataset was first clipped using the shape file covering the study area. The points have been pre-classified into four different classes: ground, water, bridges and unclassified using automated routines in TerraScan (The Swedish Land Survey, 2011). A DTM was computed using the last returns from the LiDAR points in the ground class and merged to a raster with a cell size of 3 meters. A correct cell size is important to minimize pixels with no data values in the output and a rule of thumb is to multiply the average point spacing of the LiDAR datasets (0.85 points/m^2) with four and to set the cell size to the closest integer (ESRI, 2011). The slope gradient, or the maximum rate of change from one cell to its surrounding cells in a 3 x 3 neighborhood, was calculated based on the DTM using the neighborhood slope algorithm (also refered to as the average maximum technique) (Burrough & McDonell, 1998).

A DSM was generated using the first returns (to extract only the top of the canopies) from the unclassified LiDAR points. The cell size when converting the points to a raster was set to 0.85 m based on the average LiDAR point spacing. This was done to be able to delineate individual tree canopies in the CHM that was produced. Gap filling was performed on the DEMs by giving empty cells the mean value of the surrounding pixels in a 3x3 pixel window.

The slope of the terrain, or the maximum rate of change in elevation between a pixel in the DTM and its surrounding pixels in a 3 x 3 neighborhood, was computed using the

neighborhood slope algorithm (also known as the average maximum technique) (Burrough and McDonell, 1998).

Lastly a CHM was derived by subtracting the DTM from the DSM to get a raster layer with canopy heights above ground level. All pixels below 1 m were set to 0 m to prevent very low objects, like bushes or stones, to affect the biomass estimates. The coefficient of variation (CV) was used to compare the heterogeneity of the tree heights at different parts of the forest and is the ratio between the standard deviation and mean.

3.7.2 Accuracy assessment

The root mean square error (RMSE) (Equation 7) was used to estimate the accuracy of the DTM and CHM. RMSE is a measure of the difference between observed and modelled values and can be expressed as:

$$RMSE = \sqrt{\frac{1}{N}\sum_{i=1}^{N}(x_i - \bar{x_i})^2} \qquad (7)$$

where x_i are the measured values and $\bar{x}i$ are the predicted values.

The DTM was validated with the 18 points collected in the center of each field plot. The CHM was validated by comparing the mean tree height of each field plot with the mean tree height of the CHM corresponding to the same geographic area. The RMSE of the CHM does therefore apply to the mean tree height of the plots and not individual trees.

3.8 Biomass modelling

The LiDAR dataset was clipped to 18 subsets using 200 m^2 polygons created around coordinates collected in the center of each field plot (Figure 9). The horizontal accuracy of the coordinates used pended between 1 and 30 cm according to the Topcon GRS-1 instrument. High horizontal accuracy is crucial to make sure the subsets correspond to the exact same geographic location and area as the 18 field plots.

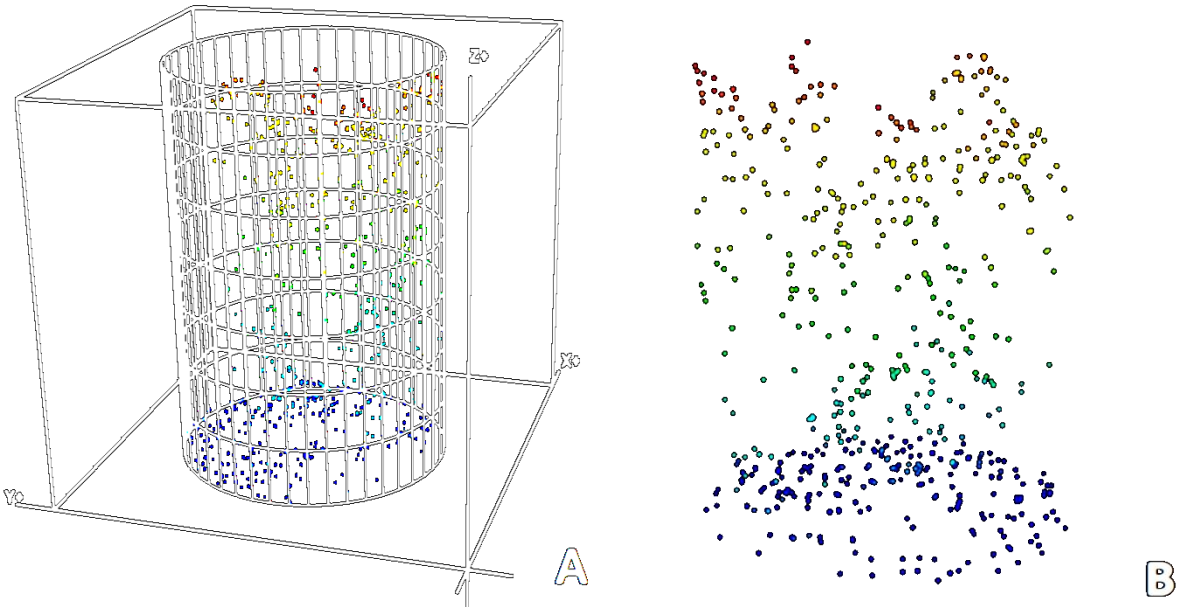

Figure 9. A: The LiDAR point cloud clipped using a cylinder with the same diameter as the field plots. B: The resulting clipped subset with the cylinder removed. The example shown is from field plot NW100.

The FUSION software was used to compute a range of plot metrics for the subsets (McGaughey and Carson, 2007). The metrics include parameters such as mean canopy height, height percentiles divided into different return numbers and a canopy cover ratio. The canopy cover ratio is estimated by taking all return values above the mean, dividing them by the total first returns and multiplying it by 100 (Equation 8) (McGaughey, 2014).

$$\frac{\text{all returns above mean}}{\text{total first returns}} * 100 \qquad (8)$$

Linear and non-linear multiple regression analysis was carried out, using the LiDAR plot metrics as predictor variables and the field plot AGB estimates as response variable. The adjusted coefficient of determination (R^2_{adj}) was used to find what predictors and types of functions were most capable of modelling AGB. The coefficient of determination (R^2) is a measure used in regression analysis to quantify the proportion of the variance in a dependent variable that is predictable from independent variables (Rao, 1973). The R^2_{adj} has been adjusted for the number of explanatory variables and observations used in the model and can be described as:

$$R^2_{adj} = 1 - \left(\frac{n-1}{n-p}\right) * \frac{SSE}{SST} \qquad (9)$$

where *n* is the number of observations, *p* is the number of regression coefficients estimated (including the intercept), SSE is the sum of squared error and SST is the sum of squared total

(Dufour, 2011). Compared to R^2, R^2_{adj} only increases if a predictor adds more explanatory power to the function than would be obtained by probability and decreases when a predictor enhances the model less than what would be expected from chance (Dufour, 2011).

The predictor variables yielding the highest R^2_{adj} were computed for the entire study area and converted to raster layers. A pixel-resolution of 14 x 14 m (196 m^2) was chosen, corresponding roughly to the size of the field plots (200 m^2). The functions yielding the highest R^2_{adj} were applied to the rasters containing the predictors resulting in a single raster layer containing the estimated AGB. The output was resampled to 25 x 25 m to be able to compare it with the SLU Forest Map. This was achieved using nearest neighbor assignment which finds the location of the closest cell center in the input raster and assigns it to the new cells in the output raster (ESRI, nd).

The field plot located 50 m north of the research tower was not used in the regression model as the LiDAR metrics showed a mean tree height of 12.5 m while the mean tree height measured in field was 4.5 m, indicating that trees have been cut or wind-thrown after the LiDAR data was collected.

4. Results & Discussion

In this section the outcome of the field measurement, land cover classification, digital elevation modelling and AGB estimates will be presented. All maps are referenced according to the SWEREF99 TM projected coordinate system and have the following extent, left: 444726, right: 4457389 top: 6243987, bottom: 6243012. The flux tower has been marked with a white star in all the maps.

4.1 Field plot measurements and reference AGB estimations

The field measurements (can be found in Appendix II) showed large variability between the different plots. The mean tree height (Figure 10) varies between 5.5 m in a young birch stand (NW200), to 21.1 m in a mature beech stand (NW325), with an average of 11.1 m and a standard deviation of 3.7 m between the plots. The standard deviation within the plots varies between 0.5 and 9.4 m. The number of trees higher than 2 m in each plot varies from 8 (NW325) to 57 (E50).

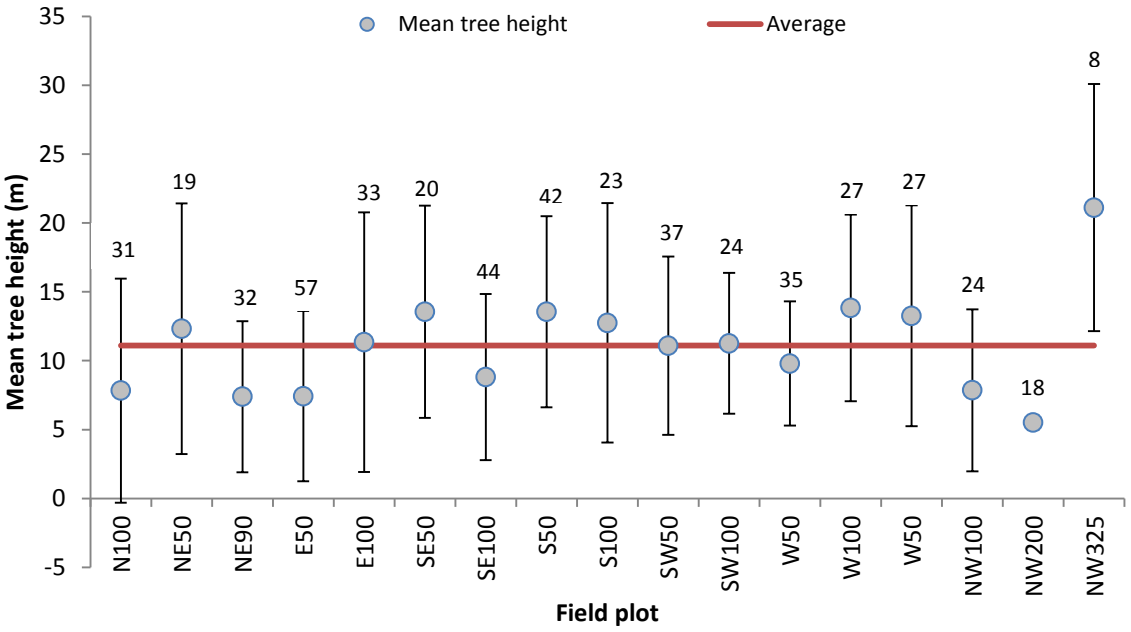

Figure 10. Mean tree height of the field plots with error bars representing +-1 standard deviation. The numbers on top of the errorbars represent the number of trees above 2 m in that field plot.

The total AGB per field plot, estimated with the functions in Table 1, was multiplied by 50 to get the AGB/ha presented in Figure 11. The AGB ranges from 2025 kg/ha (NE200) to 272 805 kg/ha (NW325) between the field plots, with an average of 147 744 kg/ha and a standard deviation of 70 417 kg/ha. Spruce is the tree species accounting for the largest part of the total AGB within the plots (56.2 %) followed by pine (16.0 %), beech (11.1 %), oak (7.5 %) and

birch (6.8 %) (Figure 12). Rowan and alder were few and only accounted for 2.5 % of the total AGB, the fact that their AGB was estimated with functions for birch and beech should therefore have a small effect on the results. Only 0.77 % of the total measured AGB comes from trees that are between 2 m and 5 m high, the decision not to measure trees less than 2 m high should therefore not have a big effect on the AGB estimates either.

Plot NW325 had the highest mean tree height, the lowest tree count and the highest AGB, indicating that mean tree height has a larger influence on the total AGB than the tree count.

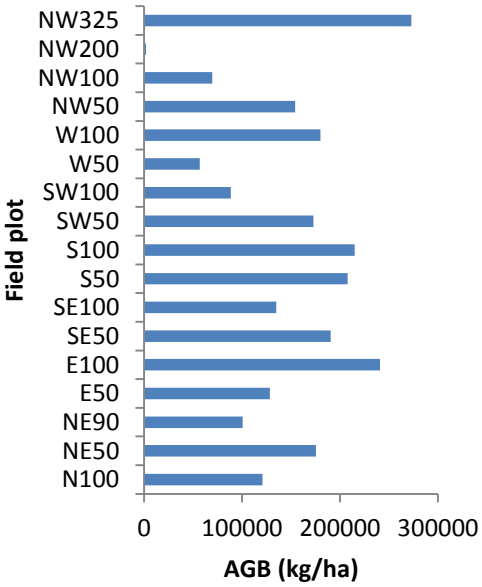

Figure 11. Total AGB (kg/ha) within the field plots (200 m^2 each).

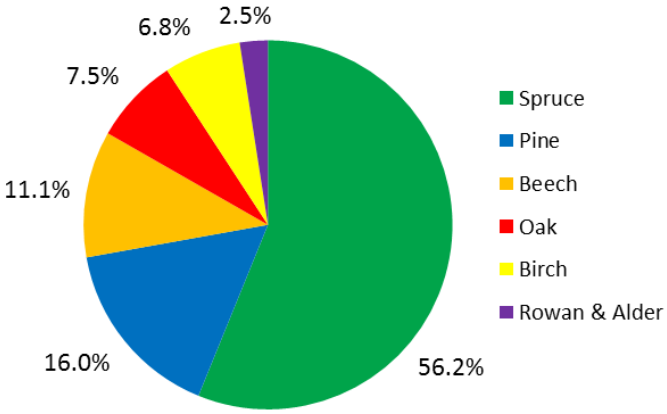

Figure 12. Distribution of AGB between different tree species within the field plots.

4.2 Land cover classification

The spectral signature of the beech and oak classes proved hard to separate with a Jeffries-Matusita Distance (JM) of 1.38 and a Transformed Divergence (TD) of 1.67. Both of these statistics have been squared to range between 0.0 and 2.0, low values indicates poor separablity, while high values demonstrate that the classes are well separated (Richards & Richards, 1999). The beech and oak classes were therefore merged into a new class called broadleaved. Spruce and pine also proved hard to separate (JM: 1.51 and TD: 1.76) but both were kept as output classes.

The pixel-based land cover classification (Figures 13 and 14) revealed a mixed forest with spruce occupying 22.1 % of the study area followed by pine (17.3 %), broadleaved trees (9.9 %), succession (8.3 %) and bare ground (6.4 %). The biggest class was shadows which was

reduced from 50.5 % to 35.9 % after replacing the shadow class with the classification based on the image from 2012.

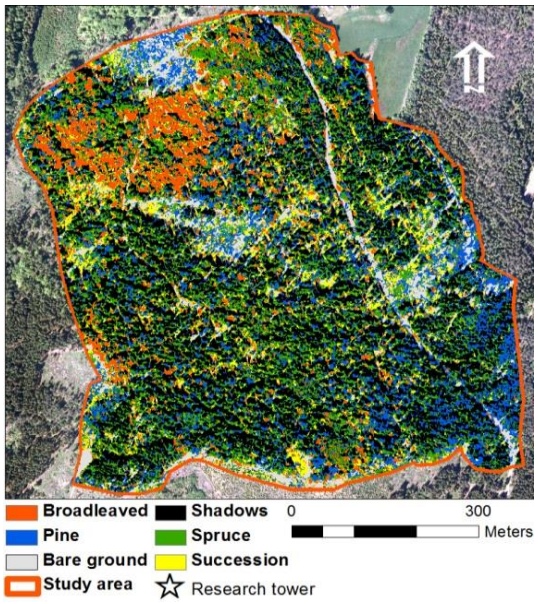

Figure 13. The resulting pixel-based land cover classification. © Kommunerna i Skåne

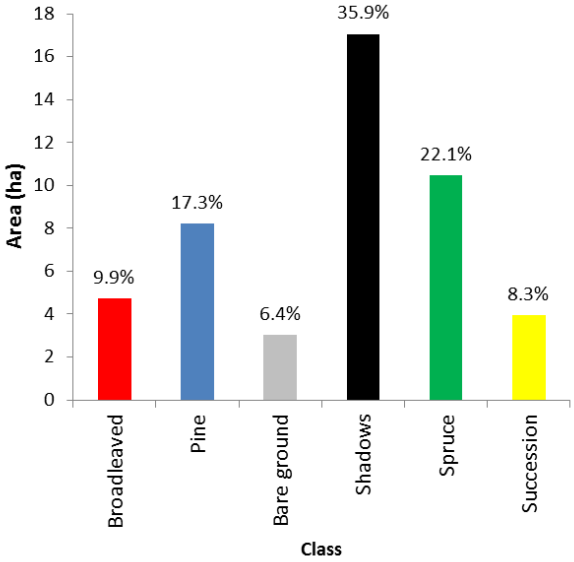

Figure 14. Distribution of classes according to the pixel-based classification.

The accuracy assessment of the pixel-based classification showed an overall accuracy of 56 % and a kappa value of 0.40, making it 40 % better than chance (Table 2). The bare ground class was overestimated with a users's accuracy of 29 % and a producer's accuracy of 100 %. The confusion matrix also shows that many pine trees were misclassified as spruce.

Table 2. Confusion matrix for the pixel-based classification. The horizontal axis represents ground truth classes based on the validation points collected in field and the vertical axis the classes assigned by the classifier.

Class	Succesion	Spruce	Broadleaved	Bare ground	Pine	Total	User's (%)	Producer's (%)
Succession	3	1	1	0	1	6	50	70
Spruce	0	32	6	0	6	44	73	48
Broadleaved	0	4	15	0	0	19	79	46
Bare ground	7	5	0	7	5	24	29	100
Pine	0	20	6	0	21	47	45	57
Total	10	62	28	7	33	140		

The results from the object-based classification approach (Figures 15 and 16) shows that spruce was by far the most dominating class (40.2 %) followed by shadows (26.6 %). Pine was the second most occurring tree species (13.8%) succeeded by broadleaved trees (8.7 %),

succession (6.7 %) and bare ground (4.1 %). The shadow class was reduced from 51.5 % to 26.6 % after shadow filling had been performed.

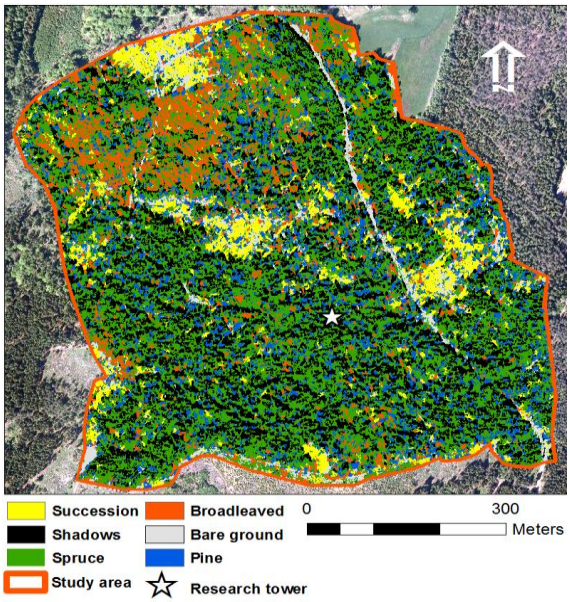

Figure 15. The result from the object-based classification approach. © Kommunerna i Skåne

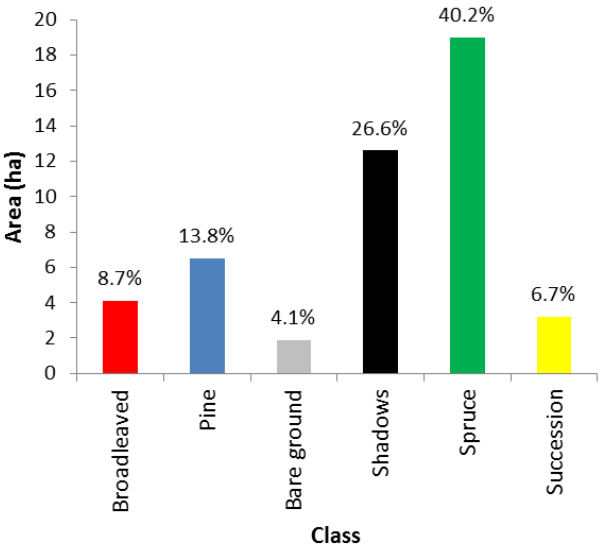

Figure 16. Distribution of land cover classes.

The accuracy assessment of the object-based classification approach (Table 3) shows an overall accuracy of 75 % and a kappa value of 0.65, making the classification 65 % better than chance. The object-based approach hence outperformed the pixel-based method which had a kappa value of 0.40. The improvement can likely be contributed to the segmentation process, reducing the variability of the pixel values and to the spectral, textural and spatial attributes used in the classification (Hsu, et al 2010). The main difference between the two classifications is that the object-based approach to a higher degree classified succession in the open areas in the northern, center and eastern parts of the study area and resulted in less overshooting of the pine class. The spruce and pine classes still proved hard to separate with producer's accuracies of 74 % and 79 % respectively. This had a big effect on the overall accuracy and kappa value of the classification.

Table 3. Confusion matrix for the object-based classification. The horizontal axis represents ground truth classes based on the validation points collected in field and the vertical axis the classes assigned by the classifier.

Class	Succesion	Spruce	Broadleaved	Bare ground	Pine	Total	User's (%)	Producer's (%)
Succession	10	1	1	0	5	17	59	100
Spruce	0	46	2	0	2	50	92	74
Broadleaved	0	2	19	0	0	21	90	68
Bare ground	0	0	0	4	0	4	100	57
Pine	0	13	6	3	26	48	54	79
Total	10	62	28	7	33	140		

Shadows, cast from e.g. topography and trees have a severe effect on high resolution images. This was especially noticeable in the image from 2010. The pNDVI reduced this effect somewhat as it compensated for extraneous factors affecting the image such as changing illumination conditions, surface slope and aspect (Tucker, 1979; Bannari et al. 1995). Shadowfree images would have made the classification process considerably easier and improved the results. Aerial images collected with a smaller solar zenith angle should be used if the aim is to classify images at this spatial resolution (25 cm). Sacrificing spatial resolution for more shadow free images might result in an overall better accuracy.

4.3 Digital terrain model

The DTM (Figures 17 and 18) reveals a complex terrain, with a ridge extending in a south-north direction. The highest areas can be found in the northern parts of the study area with a maximum elevation of 107.3 m.a.s.l. The lowest terrain can be found in the eastern parts, with a minimum elevation of 76.2 m.a.s.l. The mean elevation is 91.3 m.a.s.l. and the standard deviation 7.9 m. The research tower is located 88.1 m.a.s.l. on the eastern slope of the ridge with most of the higher areas north or northwest of the tower. However, higher areas can also be found in western and southern directions.

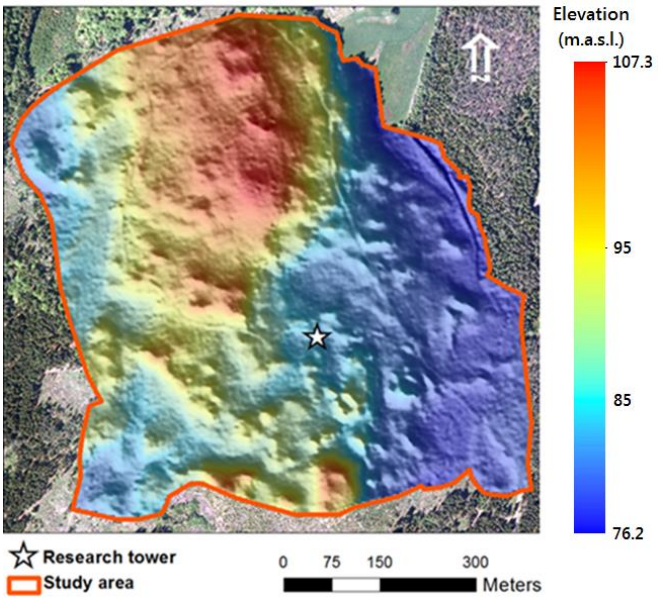

Figure 17. The DTM with a color ramp on top of a shaded relief. The shaded relief simulates cast shadows by illuminating the surface using a directional light source. © Lantmäteriet i2014/764

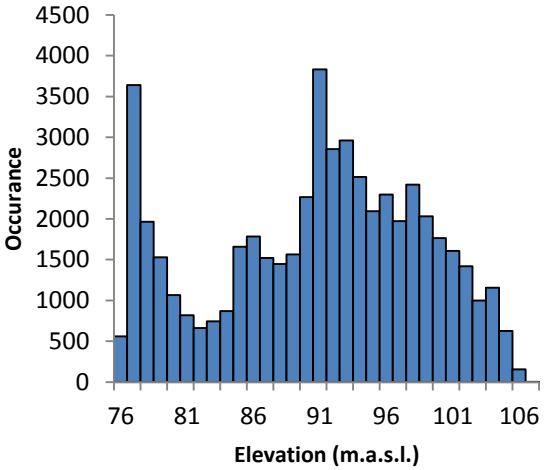

Figure 18. Histogram of the elevation values.

The steepest terrain can be found in the north-eastern and southern parts of the study area where the slope gradient is up to 34.1 % (Figure 19).

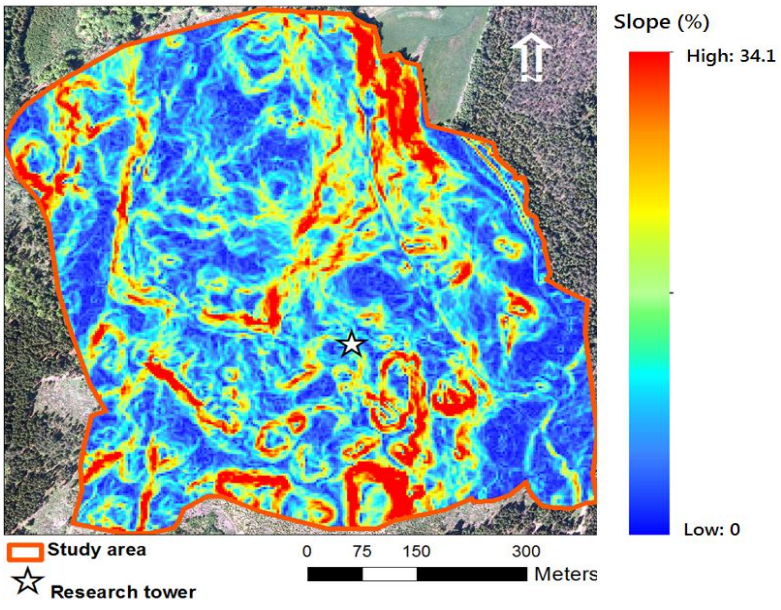

Figure 19. Steepness of the terrain in percent (the maximum rate of change between a pixel in the DTM and its surrounding pixels in a 3 x 3 neighborhood). © Lantmäteriet i2014/764

The accuracy assessment of the DTM showed a mean error of 1.1 m, an RMSE of 2.2 m and a standard deviation of 1.9 m (Figure 20 and Appendix Table 5). The lowest deviation

compared to field measured elevation points can be found in NE50 (1.17 m) and the highest in SE100 (7.15 m).

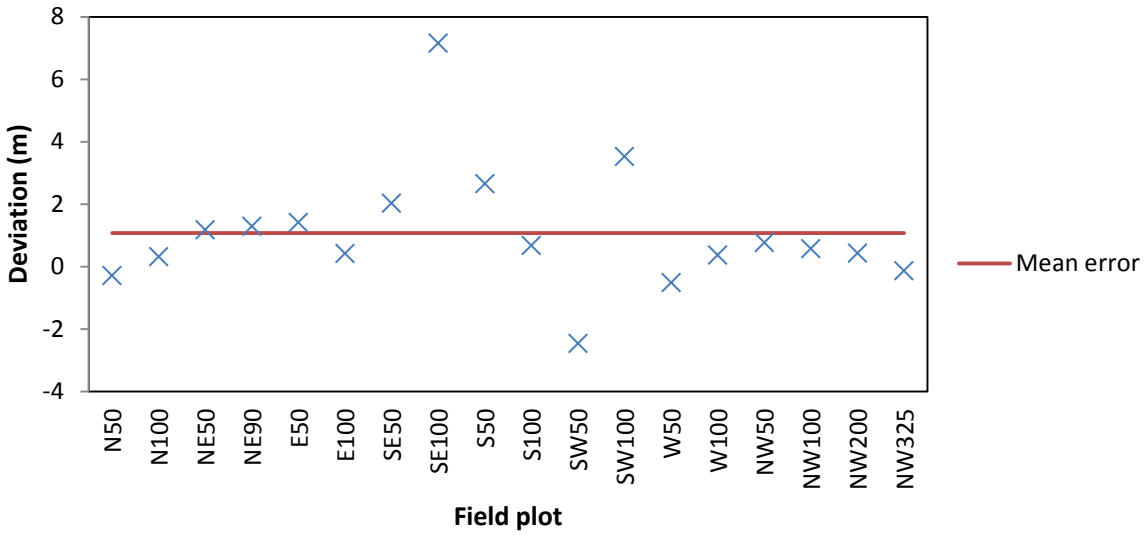

Figure 20. The deviation of the DTM in relation to field measurements. RMSE: 2.2 m.

A possible cause for the high deviation in SE100 could be that the point lies on a steep slope. The horizontal accuracy of LiDAR data is normally much lower than the vertical accuracy. In flat landscapes this is a small problem, but the effect is bigger in hilly terrain as the accuracy decreases with an increased slope (The Swedish Land Survey, 2011). SW50 is located in a very dense spruce dominated forest which could explain why it deviates -2.5 m as the point density declines with dense overstory (Hodgson & Bresnahan, 2004). Since spruce is an evergreen tree species, this still has an effect in the winter when the LiDAR data were collected.

Ideally, one would like to use many validation points when assessing the accuracy of the DTM. However, the accuracy of the original 150 validation points collected for validating the classification was considered too low and only the more exact measures from the center of each field plot could therefore be used.

4.4 Canopy height model

The CHM (Figures 21 and 22) shows a heterogeneous canopy cover throughout the study area. The maximum canopy height, and therefore the highest tree in the study area, was estimated to 34.6 m. The average canopy height was 15.1 m with a coefficient of variation (CV) of 52.3 %.

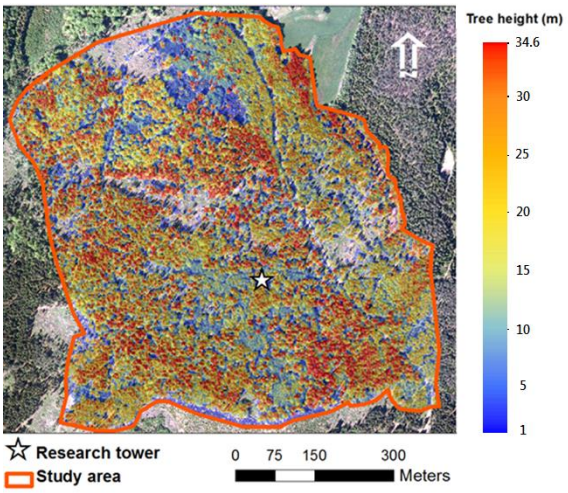

Figure 21. The CHM with 50% transperacy and a hillshade effect on top of the aerial image from 2010. © Lantmäteriet i2014/764

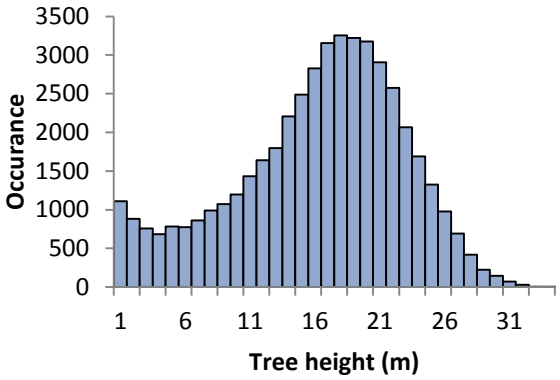

Figure 22. Histogram of the distribution of values for the CHM. The CHM has not been segmented into individual trees; the values do therefore represent pixels rather than individual trees.

The flux tower is surrounded by trees of varying height (Figure 21). High trees (above 30 m) can be found in all directions from the tower but mainly as clusters at a distance of 150 - 300 m in northern, south eastern and western directions. The height of the canopy cover closest to the tower (50 m circular radius) ranged between 1.3 and 29.0 m with an average of 15.8 m and a coefficient of variation (CV) of 35.4 %. For the annular circular section located 50 - 100 m away from the tower the canopy heights ranged between 1.0 - 29.7 m with an average of 15.9 m and a CV of 37.1 %. The most uneven part of the canopy story, in terms of height, can be found 100 - 200 m from the tower where the canopy heights vary between 1.0 to 33.2 m with an average of 16.6 m and a CV of 42.8 %. Most of the high trees can be found in the areas between 200 and 300 m from the tower, ranging between 1.0 - 33.3 m, with an average of 17.6 m and a CV of 36.4 %. Three larger (> 3000 m^2) open areas can be found in the middle, mid-eastern and north-western parts of the study area.

The accuracy assessment of the CHM (Figure 23 and Appendix II, Table 5) showed a mean error of -0.12 m, an RMSE of 3.2 m and a standard deviation of 3.3 m. The field plot with the highest deviation (-7.0 m) was NE90. NE90 is today a young birch forest stand with a few mature spruce and pine trees and it is not inconceivable that there might have been more high trees within this plot when the data was collected. These trees were likely cut or wind-felled and subsequently replaced by plant succession.

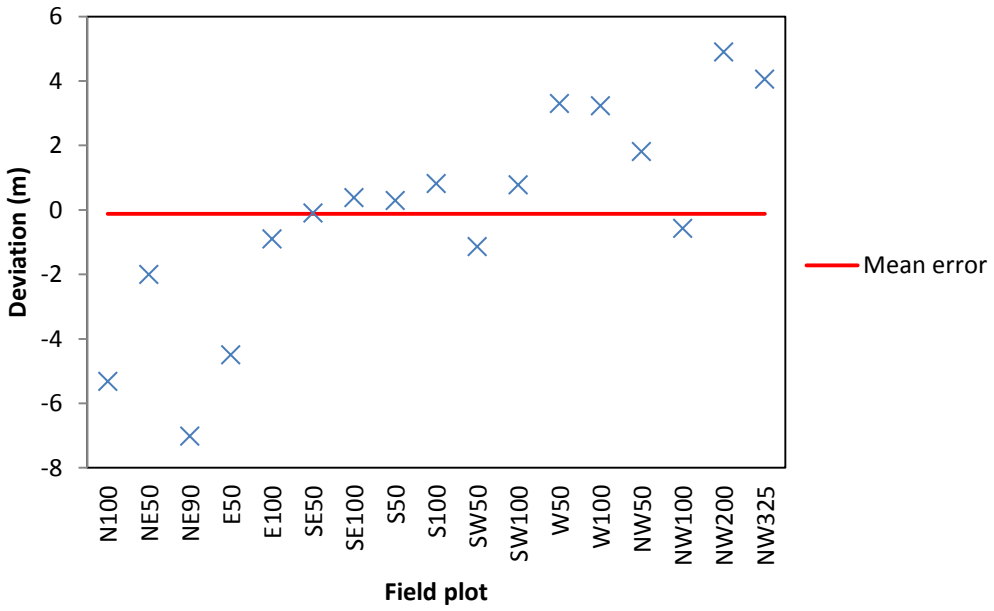

Figure 23. The deviation of the CHM in relation to measured mean tree heights. RMSE: 3.2 m.

The heterogeneity of the terrain and canopy cover surrounding the flux tower could be important to consider when analyzing data from the tower as the reliability of eddy-covariance measurements often depends on meteorological assumptions such as horizontal homogeneity and non-advective atmospheric conditions (Vesala et al, 2008). Such conditions are often violated in complex sites and there has therefore been a trend emerging in modelling the footprint of long-term accumulated eddy-covariance flux measurements using a less idealized, more realistic description of vegetation structure and topography (Sogachev et al, 2004; Gökede et al, 2006; Vesala et al, 2008; Barcza et al, 2009).

A visual comparison of the DTM (Figure 18) and the CHM (Figure 22) shows that high trees can be found at both low- and high lying terrain. The correlation between the modelled elevation above sea level of the terrain and canopy height was found to be negligible (R^2_{adj}: 0.01). Previous studies show that the relationship between local elevation differences and canopy height is stronger than between the general elevation of the terrain and canopy heights (McNab, 1989). However, although it is visually noticeable that many high trees (>30 m) are located on the steepest slopes of the terrain (e.g. in the north-eastern parts of the study area), the correlation between the modelled slope gradient and canopy height is negligible (R^2_{adj}: 0.01).

4.5 Biomass model

The regression analysis showed that the predictors able to model AGB best were the mean canopy height and the canopy cover ratio (described in section 3.8). Fitting a power function to the mean canopy heights and a linear function to the canopy cover ratio (Equation 10) resulted in the best model fit, yielding an R^2_{adj} of 0.66.

$$AGB\ (kg) = 1.567 * 10^{-11} * x^{11.34} + 62.63 * y \qquad (10)$$

where *x* is the mean tree height (m) and *y* is the canopy cover ratio.

The output from the model (Figure 24) shows that the AGB varies highly across the study area spanning from 750 kg/ha in the blue parts of the map to more than 249 700 kg/ha in the red parts. The average AGB for the entire study area was 122 900 kg/ha with a standard deviation of 50 497 kg/ha.

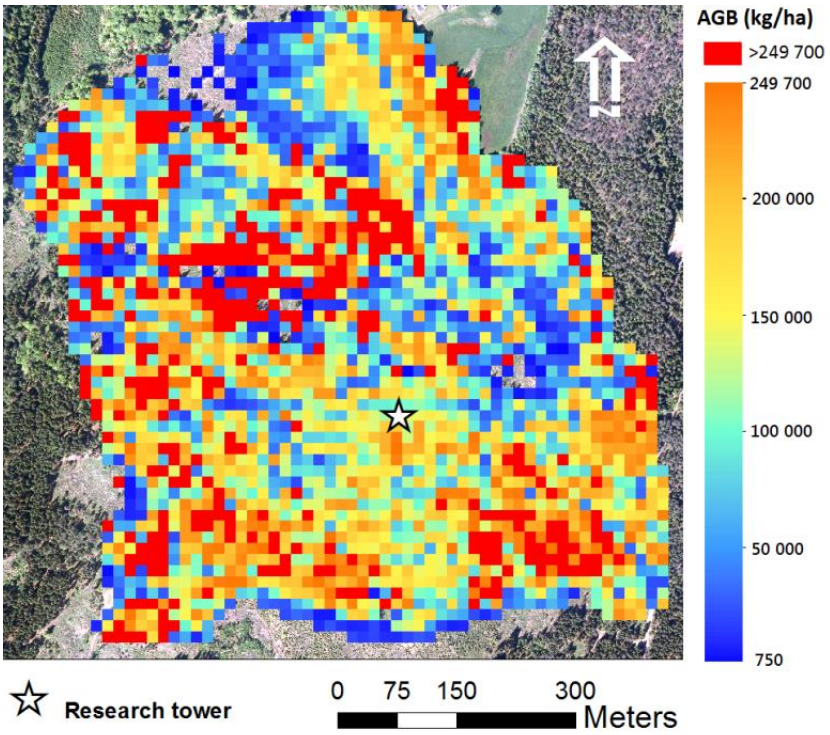

Figure 24. Modelled AGB (kg/ha) with a pixel resolution of 14 x 14 m.

It is clear that the AGB estimates are governed by the mean tree heights when comparing the CHM (Figure 21) with the modelled AGB (Figure 24). Many of the areas with the highest AGB values (>249 700 kg/ha) coincide with the areas where the highest trees are found. The high biomass northwest from the flux tower lies partly in an opening according to the aerial imagery used for the land cover classification and low AGB values were therefore expected at

this location. This can be explained by high mean tree heights in the computed metrics. These trees have been removed (cut or windfelled) in 2010 after the LiDAR data was collected but before the aerial image was taken (within a 6-month period). This was confirmed using older aerial images where the trees were present.

Three pixels had AGB values of more than 50 000 kg (2.5 million kg/ha). The cause of the outliers is the nature of the power-function, overshooting pixels with a mean tree height higher than the field plots used in the regression model (17.1 m). Since the mean tree height metric was raised by 11.34 in the power-function, the AGB of the model increase fast with increase in mean tree height. All AGB values resulting from a mean tree height above 17.1 m are represented in red in figure 27, as this was considered to be the upper limit of the model. Using a linear function would likely have resulted in more reasonable predictions for the high values but would not have been as accurate when predicting the values in the low- to medium range. Dividing the dataset and using a linear function on only the outliers would likely result in an overall more accurate model. Due to the small sample size the model should only be used on the part of Romperöd characterized by selective thinning. If one would collect more field data, the range and robustness of the model would most likely increase.

Studies have shown that the integration of optical imagery and LiDAR data can result in substantial improvements of biomass estimates compared to using LiDAR data alone (Chen et al, 2007; Cao et al, 2014). In order to fuse the two data sources, CHMs are often divided into individual tree crowns using segmentation algorithms after which allometric functions based on the relationship between tree height and AGB (Figure 25) can be applied to each tree in the study area individually (Shendryk, 2013).

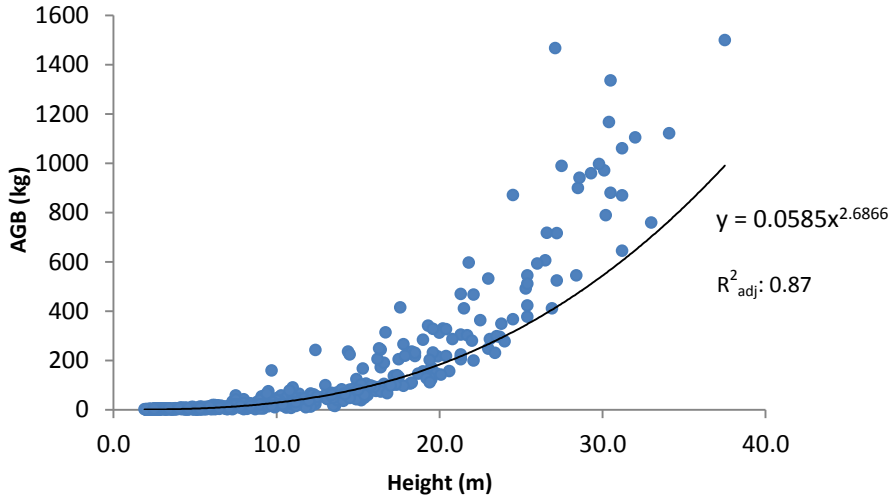

Figure 25. The relationship between measured tree heights and AGB based on all the 540 trees measured in the 17 field plots. A power function (black line) has been fitted to the data.

A power function (Figure 25) managed to describe the relationship between tree height and AGB better (R^2_{adj} of 0.87) than using for example a linear or exponential function which both yielded lower R^2_{adj} values. This is in accordance with previous studies which often make use power functions to model AGB using tree height as the only predictor (Chen et al, 2007; Shendryk, 2013). However, an attempt to isolate individual tree crowns using the watershed algorithm (Roerdink and Meijster, 2001) unfortunately produced inconsistent results due to the heterogeneity of the forest and the point density of the LiDAR data, which often was as low as 0.25 points/m^2. Since the canopy heights in Romperöd are so varied, and because trees often are standing close together, many trees are hidden by higher tree canopies. This is a problem in particular when estimating AGB based on CHMs as the interpolation process involved while creating CHMs smoothes the image, making neighboring trees inseparable (Reitberger et al, 2009). LiDAR data with a higher point density would therefore be needed for this type of analysis.

4.6 Biomass comparison

Approximately 12.6 % of the study area has a modelled AGB of more than 250 000 kg/ha. However, open areas (AGB<50 000 kg/ha) occupies 11.5 % of the study area, excluding those from the output increases the percentage of high AGB values (>250 000 kg/ha) to 14.2 %. This can be compared to a typical mixed mature (105 years old) forest, growing on medium fertile soils in the central part of Sweden where the AGB lies somewhere around 181 000

kg/ha, or to a mature (82 years old) spruce forest growing on fertile soils in southern Sweden, where the AGB typically amounts to approximately 277 000 kg/ha (Kunskap Direkt, 2015).

The total AGB of the study area was modelled to 7 129 079 kg (5 771 465 kg when the CHM was restricted to a maximum height of 17.1 m) which is considerably lower than the total AGB when upscaling the field plots (123 322 279 kg). This can be contributed to the fact that the model based on the LiDAR data successfully predicts low AGB in areas with low canopy heights which the upscaling based on the field plots does not.

The SLU Forest map differs greatly from the modelled AGB with a total AGB of 1 949 000 kg and an average of 140 469 kg/ha for the entire study area compared to the modelled total of 5 771 465 kg and average of 122 900 kg/ha. The spatial distribution of the modelled AGB and the AGB from the SLU Forest map do not coincide (Figure 26). As an example, the SLU Forest Map shows low and even no AGB in the mature broadleaved forest northwest from the flux tower where high values were modelled (and should be expected). This is in accordance with a previous study which concluded that the SLU Forest Map show relatively large estimation errors on a stand level (Blomberg, 2010).

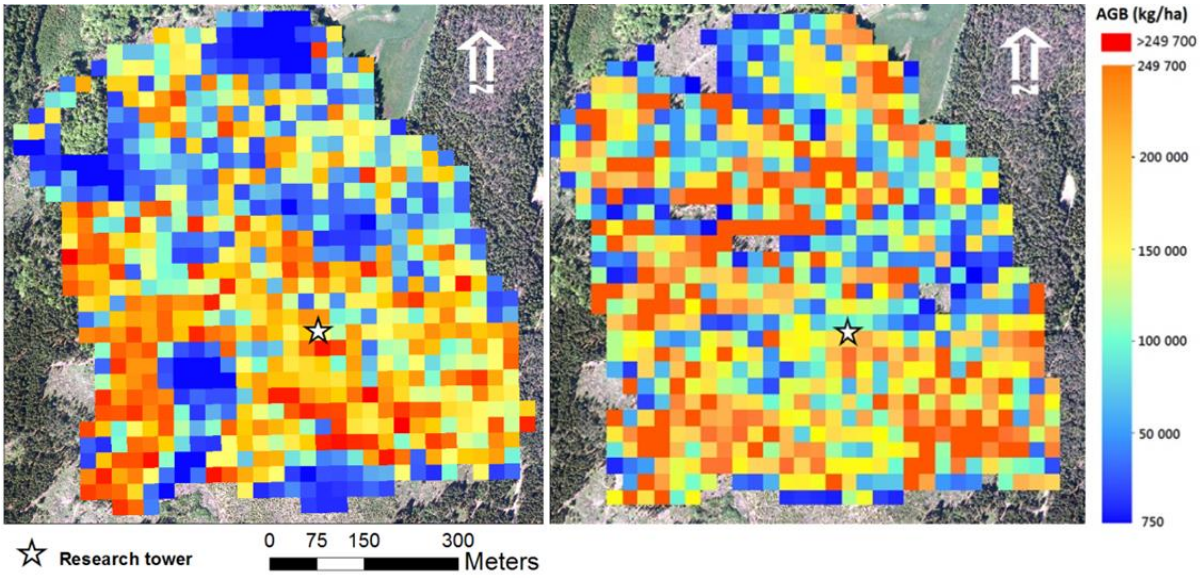

Figure 26. To the left, AGB (kg/ha) according to the SLU Forest Map. Source: SLU Forest Map, Dept. of Forest Resource Management, Swedish University of Agricultural Sciences. To the right, the modelled AGB resampled to the same pixel-resolution (25 x 25 m) with a matching color ramp.

The correlation between the modelled AGB and the AGB of the SLU Forest Map is negligible with an R^2_{adj} of 0.01 (Figure 27).

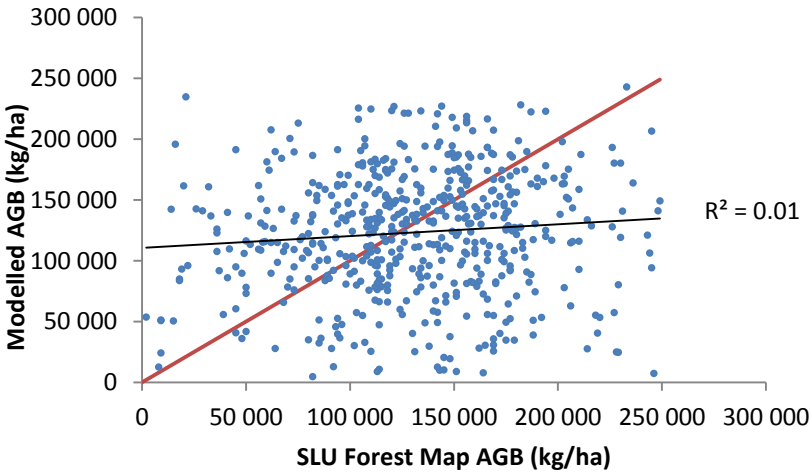

Figure 27. Modelled AGB VS SLU Forest Map AGB. Only values within the range of the model (750 – 250 000 kg/ha) were compared. A 1:1 line (red) and a fitted linear regression line (black) have been added.

When comparing the modelled AGB and the AGB from the SLU Forest Map with AGB estimated from field measurements (Figure 28) it is evident that the model developed outperforms the SLU Forest Map with R^2_{adj} values of 0.70 and 0.14 respectively. SLU states in the description of the data that it is intended for larger areas and that it should be used with caution if the study area is less than a couple of hundred hectares. The study area in this thesis covers only 47.5 hectares and does therefore not meet these requirements.

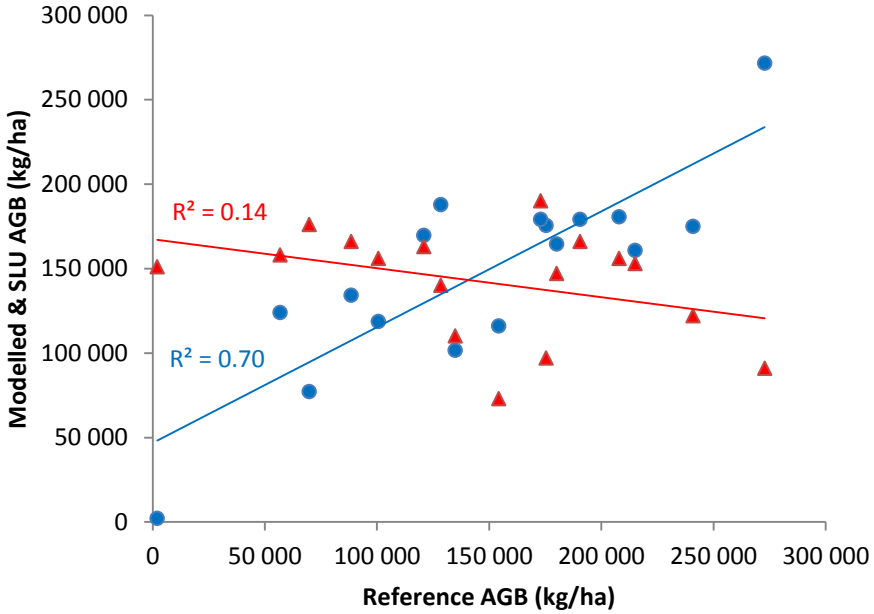

Figure 28. Modelled AGB (blue circles) and SLU Forest Map AGB (red triangles) VS reference AGB based on field measurements. Fitted linear functions (blue & red lines) have been added to compare the correlation.

The model was validated using the field plots used in the regression analysis. Additional field plots should be collected for an objective accuracy assessment but measuring tree heights is time consuming. A solution would be to only measure DBH as there are allometric functions where it is the only variable needed for estimating AGB (Johansson, 1999). This would increase the speed of measuring field plots considerably.

4.7 Further scope

For further, more detailed, remote sensing studies of Romperöd, or forests with similar characteristics, new more detailed LiDAR data should be acquired. High resolution multispectral images with a solar zenith angle close to zero could be collected in the same flight to minimize the effects of shadows and in that way allow for a more complete land cover classification. More field plots should be measured for more robust and accurate AGB estimates and to validate the results objectively.

Additional remote sensing studies of Romperöd could include forest health assessments to investigate what effects the forestry in Romperöd has on the forest health compared to other forestry methods. Multispectral data including the red-edge band would be suitable for this type of study as the red-edge band is particularly good at detecting changes in chlorophyll content. Examples of high resolution satellite systems including this band are the RapidEye, WorldView-2, or the WorldView-3 launched in August 13th, 2014 (DigitalGlobe, nd).

5. Conclusions

The land cover classification showed that the forest in Romperöd is mixed regarding the coverage of different tree species. The object-based classification approach resulted in more accurate maps than the pixel-based approach with kappa values of 0.4 and 0.65 respectively. This proves the importance of segmentation and including spectral, textural and spatial attributes when classifying complex study areas, like heterogeneous forests. Most of the different land cover types occurring in the study area were classified with satisfying results but it proved hard to distinguish between English oak and European beech, which therefore were merged into a single class. Norway spruce and Scots pine were also problematic to separate but were kept as output classes with producer's accuracies of 74 % and 79 % respectively.

The terrain of the study area is hilly with a ridge extending from south to north, an average elevation of 76.2 m.a.s.l. and a standard deviation of 7.9 m. The canopy height varies greatly across the whole study area with an average height of 15.1 m and a CV of 52.3 %. The flux tower is located 88.1 m.a.s.l. on the eastern slope of the ridge and is surrounded by a vertically heterogenous canopy cover.

The AGB estimates based on a combination of LiDAR data included in the national elevation model and field measurements outperformed the SLU Forest Map with R^2_{adj} values of 0.70 and 0.14 respectively when evaluated against estimates based on field measurements. This shows that the SLU Forest Map is unsuitable for the part of the Romperöd forest characterized by selective thinning. The LiDAR data improved the level of detail of the AGB estimates compared to when upscaling AGB estimates based solely on field measurements. However, the data was not detailed enough to delineate individual tree crowns in the study area. Being able to do so is particularly important in a heterogeneous forest like Romperöd as AGB may have high spatial variance compared to homogeneous forests where upscaling field plots might yield acceptable results. The inclusion of higher resolution LiDAR data, where individual canopies could be separated, would further improve the AGB estimates as it would make it possible to apply species-specific allometric functions to each tree in the study area individually based on the land cover classification.

Remote sensing proved to be a valuable complement to field-based forest inventories. The methodology used can be applied in forest management planning or to monitor future changes

to the carbon stock of the forest. The characterization may aid in further studies regarding the Romperöd forest and its carbon exchange with the atmosphere.

Acknowledgements

I would like to give special thanks to my supervisors, Niklas Boke-Olén and Patrik Vestin at the Department of Physical Geography and Ecosystem Science, Lund University, for expert advice and guidance. I am also grateful to David Göransson, the forest owner, for taking me on a field trip to Romperöd and allowing me to conduct field measurements there. I would also like to thank Andreas Persson and Fredrik Lagergren for providing field equipment and Liisi Nõgu for showing me the locations of the previous field plots and how they were measured.

My final, but equally important, gratitudes go to my family, friends and to Lina Staffansdotter, for their encouragement and support when the going got tough.

References

Andersson, E. 2006. Alternativa skogsbruksmetoder i Norden. PhD Thesis. Swedish University of Agricultural Sciences, Umeå.

Baltsavias, E.P. 1999. Airborne laser scanning: Existing systems, firms, and other resources. *ISPRS Journal of Photogrammetry and Remote Sensing* 54: 164-198.

Bannari, A., D. Morin, F. Bonn, and A.R. Huete. 1995. A review of vegetation indices. *Remote Sensing Reviews* 13: 95–120.

Barcza, Z., Kern, A., Haszpra, L., and N. Kljun. 2009. Spatial representativeness of tall tower eddy covariance measurements using remote sensing and footprint analysis. *Agricultural and Forest Meteorology* 149: 795-807.

Blaschke, T. 2003. Object-based contextual image classification built on image segmentation. *Advances in Techniques for Analysis of Remotely Sensed Data, IEEE Workshop*: 113-119.

Blomberg, R. 2010. Tillämpning av kNN-Sverige i Södra Skogs verksamhet: behovsinventering, databearbetning och förberedelse för praktisk implementering. Master Thesis. Swedish University of Agricultural Sciences, Umeå.

Boser, B., I. Guyon, and V. Vapnik. 1992. A training algorithm for optimal margin classifiers. *Proceedings of the Fifth Annual ACM Workshop on Computational Learning Theory*.

Brandini, P. and G. Tabacchi. 1996. Biomass and volume equations for holm oak and straberry-tree in coppice stands of Southern Sardinia. *ISAFA communicazionidi Ricerca* 96: 59–69.

Burba, G. 2013. Eddy Covariance Method for Scientific, Industrial, Agricultural and Regulatory Applications: A Field Book on Measuring Ecosystem Gas Exchange and Areal Emission Rates. Li-Cor Biosciences.

Burrough, P. A. & R. A. McDonell. 1998. Principles of Geographical Information Systems. Oxford University Press, New York, 190 pp.

Cao, L., N. C. Coops, T. Hermosilla, J. Innes, J. Dai & G. She. 2014. Using small-footprint discrete and full-waveform airborne LiDAR metrics to estimate total biomass and biomass components in subtropical forests. *Remote Sensing* 6: 7110-7135.

Carey, A. B., M. M. Hardt, S. P. Horton & B. L. Biswell. 1991. Spring bird communities in the Oregon coast range. USDA Forest Service, general technical report PNW-GTR-285. Pacific Northwest Research Station, USA.

Chen, Q., Gong, P., Baldocchi, D., & Tian, Y. Q. 2007. Estimating basal area and stem volume for individual trees from lidar data. *Photogrammetric Engineering & Remote Sensing* 73: 1355-1365.

Chu, T., and X. Guo. 2014. Remote sensing techniques in monitoring post-fire effects and patterns of forest recovery in boreal forest regions: A review. *Remote Sensing* 6: 470–520.

Cohen, J. 1960. A coefficient of agreement for nominal scales. *Educational and Psychological Measurement* 20: 37-46.

Cortes, C., and V. Vapnik. 1995. Support-vector networks. *Machine learning* 20: 273-297.

Couteron, P., N. Barbier, C. Proisy, R. Pélissier, and G. Vincent. 2012. Linking remote-sensing information to tropical forest structure: The crucial role of modelling. *Earthzine* 4: 1-4.

de Tanago, J.G., S. Joshep, M. Herold, R. Goodman, V. Abitabile, H. Bartholomeus, and J. Janovec. 2014. Terrestrial LiDAR and 3D tree reconstruction modeling for quantification of biomass loss and characterization of impacts of selective logging in tropical forest of Peruvian Amazon. ForestSAT2014 Open Conference System.

Exelis Visual Information Solutions (VIS). 2007. An interval based attribute ranking technique. Unpublished report (retrieved from technical support, Exelis VIS).

Foody, G. M. 2002. Status of land cover classification accuracy assessment. *Remote sensing of environment* 80: 185-201.

Gibbs, H. K., S. Brown, J. O. Niles and J. A. Foley. 2007. Monitoring and estimating tropical forest carbon stocks: making REDD a reality. *Environmental Research Letters* 2: 045023.

Goetz, S. J., A. Baccini, N. T. Laporte, T. Johns, W. Walker, J. Kellndorfer & M. Sun. 2009. Mapping and monitoring carbon stocks with satellite observations: a comparison of methods. *Carbon balance and management* 4: 2.

Hese, S., W. Lucht & C. Schmullius. 2005. Global biomass mapping for an improved understanding of the CO_2 balance - the Earth observation mission carbon-3D. *Remote Sensing of Environment* 94: 94 – 104.

Hochbichler, E. 2002. Vorläufige Ergebnisse von Biomasseninventuren in Buchen- und Mittelwald-beständen. Inventur von Biomasse- und Nährstoffvor-räten in Waldbeständen. *Forstliche Forschungsberichte, München* 186: 37–46.

Hodgson, M. E., and P. Bresnahan. 2004. Accuracy of airborne LIDAR-derived elevation. *Photogrammetric Engineering & Remote Sensing* 70: 331-339.

Holmgren, J., Å. Persson, and U. Söderman. 2008. Species identification of individual trees by combining high resolution LiDAR data with multi-spectral images. *International Journal of Remote Sensing* 29: 1537-1552.

Houghton, R. A. 2005. Aboveground Forest Biomass and the Global Carbon Balance. *Global Change Biology* 11: 945 – 958.

Hyde, P., R. Nelson, D. Kimes, and E. Levine. 2007. Exploring LiDAR–RaDAR synergy-Predicting aboveground biomass in a southwestern ponderosa pine forest using LiDAR, SAR and InSAR. *Remote Sensing of Environment* 106: 28-38.

IPCC, 2014: Edenhofer, O., R. Pichs-Madruga, Y. Sokona, E. Farahani, S. Kadner, K. Seyboth, A. Adler, I. Baum, et al. 2014. Climate change 2014: Mitigation of climate change. Contribution of Working group III to the Fifth Assessment Report of the Intergovernmental Panel on Climate Change. Cambridge University Press, Cambridge, United Kingdom and New York, NY, USA.

Jin, X. 2012. Segmentation-based image processing system. U.S. Patent 8, 260, 048, filed Nov. 14, 2007, and issued Sept. 4, 2012.

Johansson, T. 1999. Biomass equations for determining functions of pendula and pubescent birches growing on abandoned farmland and some practical implicatons. *Biomass and Bioenergy* 16: 223–238.

Kangas, A. And M. Maltamo. Eds. 2006. *Forest inventory: methodology and applications.* Vol. 10. Springer Science & Business Media.

Lavrov, A., A.B Utkin, R. Vilar, and A. Fernandes. 2003. Application of lidar in ultraviolet, visible and infrared ranges for early forest fire detection. *Applied Physics B* 76: 87-95.

Leverin, M. 2014. Skogsbrukets påverkan på artmångfalden hos mossor och lavar : Är artmångfalden större i en skog vid kontinuitetsskogsbruk än vid trakthyggesbruk? Bachelor's Thesis. Skövde, Sweden: University of Skövde.

Lefsky, M. A., D. Harding, W. B. Cohen & G. G. Parker. 1999. Surface lidar remote sensing of the basal area and biomass in deciduous forests of eastern Maryland, USA. *Remote Sensing of Environment* 67: 83-98.

Lillesand, T. M., Kiefer, R. W., & Chipman, J. W. 2008. Remote sensing and image interpretation. New York: Wiley, cop.

Loveland, T. R., J.W Merchant, D.O Ohlen, and J.R. Brown. 1991. *Photogrammetry and Remote Sensing* 57: 1453-1463.

Lu, D., and Q. Weng. 2007. A survey of image classification methods and techniques for improving classification performance. *International journal of Remote sensing* 28: 823-870.

Lüthi, D., Le Floch, M., Bereiter, B., Blunier, T., Barnola, J. M., Siegenthaler, U. & Stocker, T. F. 2008. High-resolution carbon dioxide concentration record 650,000–800,000 years before present. *Nature* 453: 379-382.

MacArthur, R. H. & J. W. MacArthur. 1961. On bird species diversity. *Ecology* 50: 594-598.
Malhi, Y., P. Meir, and S. Brown. 2002. Forests, carbon and global climate. *Philosophical Transactions of the Royal Society of London* 360: 1567-1591.

Marklund, L. G. 1988. Biomass functions for Scots pine, Norway spruce and birch (Betula verrucosa [B. pendula] and B. pubescens) in Sweden. Swedish University of Agricultural Sciences, Report 45: 1-73.

McGaughey, R. J., and W.W. Carson. 2003. Fusing LIDAR data, photographs, and other data using 2D and 3D visualization techniques. Proceedings of Terrain Data: Applications and Visualization – Making the Connection. *American Society for Photogrammetry and Remote Sensing*: 16-24.

McNab, W. H. 1989. Terrain shape index: quantifying effect of minor landforms on tree height. *Forest Science* 35: 91-104.

Melgani, F., L. Bruzzone. 2004. Classification of hyperspectral remote sensing images with support vector machines. *Geoscience and Remote Sensing, IEEE Transactions* 42: 1778-1790.

Mitchard, E. T. A., S. Saatchi, L. J. T. White, K. A. Abernethy, K. J. Jeffery, S. L. Lewis & P. Meir. 2012. Mapping tropical forest biomass with radar and spaceborne LiDAR in Lopé National Park, Gabon: overcoming problems of high biomass and persistent cloud. *Biogeosciences* 9: 179-191.

Mäkiranta, P., T. Riutta, T. Pentillä, and K. Minkkinen. 2010. Dynamics of net ecosystem CO_2 exchange and heterotrophic soil respiration following clearfelling in a drained peatland forest. *Agricultural and Forest Meteorology* 150: 1585-1596.

Nelson, R., R. Oderwald & T. G. Gregoire. 1997. Separating the ground and airborne laser sampling phases to estimate tropical forest basal area, volume, and biomass. *Remote Sensing of Environment* 60: 311-326.

Nielsen, M. M. 2014. Inferring Land Use from Remote Sensing Imagery. A context-based approach. PhD Thesis. Stockholm, Sweden: Stockholm University.

Nilsson, M. 1996. Estimation of tree heights and stand volume using an airborne lidar system. *Remote Sensing of Environment* 56: 1-7.

Olsson, M. 2010. Skogsbrukets bidrag till ett bättre klimat. *Kungl. Skogs- och Lantbruksakademiens Tidskrift* 4: 7-15

Pal, M., and P. M. Mather. 2005. Support vector machines for classification in remote sensing. *International Journal of Remote Sensing* 26: 1007-1011.

Pan, Y. 2011. A Large and Persistent Carbon Sink in the World's Forests. *Science* 333: 988. DOI: 10.1126/science.1201609.

Paul-Limoges, E., T. A. Black, A. Christen, Z. Nesic and R. S. Jassal. 2015. Effect of clearcut harvesting on the carbon balance of a Douglas-fir forest. *Agricultural and Forest Meteorology* 203: 30-42.

Pirotti, F. 2011. Analysis of full-waveform LiDAR data for forestry applications: a review of investigations and methods. *Forest-Biogeosciences and Forestry* 4: 100.

Ranson, K. J., K. Kovacs, G. Sun and V. I. Kharuk. 2003. Disturbance recognition in the boreal forest using radar and Landsat-7. *Canadian journal of remote sensing* 29: 271-285.

Rao, C. R. 1973. Linear Statistical Inference and its Applications, 2nd ed. New York: Wiley.

Reich, P.B. 2011. Biogeochemistry: Taking stock of forest carbon. *Nature Climate Change* 1: 346–347. DOI:10.1038/nclimate1233

Reitberger, J., P. Krzystek and U. Stilla. 2009. Benefit of airborne full waveform lidar for 3D segmentation and classification of single trees. In *ASPRS 2009 Annual Conference:(on CD-ROM).*

Richards, J. A. & J. A. Richards. 1999. *Remote Sensing Digital Image Analysis*. Vol. 3. Berlin et al.: Springer.

Robinson, D. J., N. J. Redding, and D. J. Crisp. 2002. Implementation of a fast algorithm for segmenting SAR imagery. Scientific and Technical Report. Australia: Defense Science and Technology Organization.

Robinson, C., S. Saatchi, M. Neumann & T. Gillespie. 2013. Impacts of spatial variability on aboveground biomass estimation from L-band radar in a temperate forest. *Remote Sensing* 5: 1001-1023.

Roerdink, J.B.T.M., and A. Meijster. 2001. The watershed transform: definitions, algorithms and parallelization strategies. *Fundamenta Informaticae* 41: 187–228.

Schlesinger, W.H. 1991. Biogeochemistry: an analysis of global change. *Geological Magazine* 135: 819-842.

Schwarz, R. 2012. Development of an illumination simulation software for the Moon's surface: An approach to illumination direction estimation on pictures of solid planetary surfaces with a significant number of craters. Master's Thesis. German Aerospace Center (DLR): Merseburg University of Applied Sciences.

Shendryk, I. 2013. Integration of LiDAR data and satellite imagery for biomass estimation in conifer-dominated forest. Master's Thesis. Lund, Sweden: Lund University.

Sogachev, A., Ü. Rannik, and T. Vesala. 2004. Flux footprints over complex terrain covered by heterogeneous forest. *Agricultural and Forest Meteorology* 127: 143-158. DOI: http://dx.doi.org/10.1016/j.agrformet.2004.07.010.

Strandberg, H. 2010. Produktbeskrivning - ORTOFOTO Skåne.© *Kommunerna i Skåne*

The Swedish Land Survey. 2011. Produktbeskrivning - version 1.6. © *Lantmäteriet i2014/764*

The Swedish Land Survey. 2012. Produktbeskrivning: GSD-Ortofoto och GSD-Ortofoto tätort © *Lantmäteriet i2014/764*

Tobin, B., and M. Nieuwenhuis. 2007. Biomass expansion factors for Sitka spruce (Picea sitchensis (Bong.) Carr.) in Ireland. *European Journal of Forest Research* 126: 189-196.

Tucker, C.J. 1979. Red and photographic infrared linear combination for monitoring vegetation. *Remote Sensing of Environment* 8: 127–150.

Van Leeuwen, M., and M. Nieuwenhuis. 2010. Retrieval of forest structural parameters using LiDAR remote sensing. *European Journal of Forest Research* 129: 749-770.

Vesala, T., N. Kljun, Ü. Rannik, J. Rinne, A. Sogachev, T. Markkanen, K. Sabelfeld, Th. Foken, et al. 2008. Flux and concentration footprint modelling: State of the art. *Environmental Pollution* 152: 653–666.

Weishampel, J. F., J.B Blair, R.G Knox, R. Dubayah, and D.B Clark. 2000. Volumetric LiDAR return patterns from an old-growth tropical rainforest canopy. *International Journal of Remote Sensing* 21: 409−415.

Online resources

Albrektson, A., B. Elfving, L. Lundqvist, E. Valinger & E.V. Skogsstyrelsen. 2012. Skogsskötselserien–Skogsskötselns grunder och samband. Retreived April 15th, 2015 from http://www.skogsstyrelsen.se/Global/PUBLIKATIONER/Skogsskotselserien/PDF/01-skogsskotselns%20grunder%20och%20samband%20121204.pdf

Clark Labs. 2009. Segmentation and Segment-Based Classification. IDRISI Focus Paper. Retrieved 11 February 11th, 2015, from http://www.clarklabs.org/applications/upload/Segmentation-IDRISI-Focus-Paper.pdf

DigitalGlobe. nd. WorldView-3. Retreived April 13th, 2015, from https://www.digitalglobe.com/about/our-constellation

Dufour, J. M. 2011. Coefficients of determination. McGill University. Retrieved March 23rd , 2015, from http://www2.cirano.qc.ca/~dufourj/Web_Site/ResE/Dufour_1983_R2_W.pdf

ESRI. nd. ArcGis: Desktop 9.3 Help. Retreived May 21st, 2015, from http://webhelp.esri.com/arcgisdesktop/9.3/index.cfm?TopicName=Cell%20size%20and%20resampling%20in%20analysis

ESRI. 2011. LiDAR Analysis in ArcGIS®10 for Forestry Applications. Retrieved May 25th, 2015, from http://www.esri.com/library/whitepapers/pdfs/LiDAR-analysis-forestry-10.pdf

ESRI. 2012. Evaluating Classes and Clusters. ArcGIS Desktop Help 9.3. Retreived April 23rd, 2015, from http://webhelp.esri.com/arcgisdesktop/9.3/index.cfm?TopicName=Evaluating%20classes%20and%20clusters

Exelis Visual Information Solutions (VIS). 2015a. Optimized Linear Stretch. Using ENVI. Retrieved March 29th, 2015, from http://www.exelisvis.com/docs/BackgroundOptimizedLinearStretch.html

Göransson, D. 2015. Forest-owner. http://www.skogsstyrelsen.se/en/Projektwebbar/Baltic-Landscape/The-Sites/The-River-Helge-a/

Hsu, C.W., C.C. Chang, and C.J. Lin. 2010. A practical guide to support vector classification. National Taiwan University. Retrieved February 14th, 2015, from http://ntu.csie.org/~cjlin/papers/guide/guide.pdf

Kunskap Direkt. 2015. Hur mycket energi finns det i skogsbestånd på ett hektar? Retrieved May 10th, 2015, from http://www.kunskapdirekt.se/sv/KunskapDirekt/skogsbransle/Energi-fran-skog/Hur-mycket-energi-finns-det-i-skogen/

Law 2008:662. Forestry act §10. Retrieved April 25th, 2015, from http://www.skogsstyrelsen.se/Global/PUBLIKATIONER/svl/4645803-5de4e4-SVL_2012.pdf

Lundqvist, L., J. Cedergren & L. Eliasson. 2009. Skogsskötselserien nr 11, Blädningsbruk. Skogsstyrelsens förlag, Jönköping. Retreived May 21st 2015 from http://www.skogsstyrelsen.se/skogsskotselserien

McGaughey, R.J. 2014. USDA Forest Service, FUSION manual, version 3.42. Retrieved January, 16th, 2015, from http://forsys.cfr.washington.edu/fusion/FUSION_manual.pdf

Muise, A. 2011. Raster Image Processing Tips and Tricks - Part 4: Image Classification. ArcGIS Resources. Retrieved January 26th, 2015, from http://blogs.esri.com/esri/arcgis/2011/01/10/georef4/

Oleskog, G., K. Nilsson, and P-E. Wikberg P-E. 2008. Kontinuitetskogar och kontinuitetskogsbruk. Skogsstyrelsen Rapport 22, Jönköping. Retrieved April 27th, 2015, from http://www.skogsstyrelsen.se/Global/myndigheten/Projekt/kontinuitetsskog%20och%20hyggesfritt/Rapport_22_2008_Kontinuitetsskogar%20och%20kontinuitetsskogsbruk_Slutrapport%20f%C3%B6r%20delprojekt%20sk%C3%B6tsel_hyggesfritt%20skogsbruk.pdf

SGU (The Geological Survey of Sweden). 2015. Map viewer. Retrieved January 15th, 2015, from http://apps.sgu.se/kartvisare/kartvisare-index-en.html

SLU. 2013. National forest inventory. Retreived May, 17th, 2015 from http://www.slu.se/sv/om-slu/fristaende-sidor/aktuellt/alla-nyheter/2013/1/blandskog-ett-mangfacetterat-begrepp/?utm_source=apsis-anp-3&utm_medium=email&utm_content=unspecified&utm_campaign=unspecified

SLU. 2015. Forest Map (kNN-Sweden). Retrieved April 23rd, 2015, from skogskarta.slu.se

Swedish Environmental Protection Agency. 2015. National Inventory Report 2015. Retrieved April 21st, from http://www.naturvardsverket.se/upload/sa-mar-miljon/statistik-a-till-o/vaxthusgaser/2015/rapport-nir-2015-preliminar.pdf

Södra. 2011. Slutavverkning. Retreieved May 27th, 2015 from http://skog.sodra.com/sv/Bruka-Skog/Slutavverkning/

The Swedish Forest Agency. 2014. Skogsstatistiska årsboken 2014. Retrieved May 21st, 2015, from

http://www.skogsstyrelsen.se/Global/myndigheten/Om%20oss/%C3%85rsredovisningar/%C3%85rsredovisning%202013.pdf

The Swedish Forest Agency. 2002. Skogsvårdsorganisationernas utvärdering av skogspolitikens effekter. SUS 2001 (Meddelande I – 2002). Skogsstyrelsens förlag, Jönköping. Retrieved March, 22nd, 2015, from http://shop.skogsstyrelsen.se/shop/9098/art61/4645961-0b0ef8-1544.pdf

The World Bank. 2015. World Development Indicators - CO_2 emissions (kt). Retreived April 15th from http://data.worldbank.org/indicator/EN.ATM.CO2E.KT

Topcon. 2009. GRS-1 Operator's Manual. Retrieved February 13th, 2015, from http://www.clevutil.com/gis/GPS%5CGRS-1_OM.pdf

UN-REDD. Nd. The United Nations Collaborative Programme on Reducing Emissions from Deforestation and Forest Degradation in Developing Countries. Retrieved May 13th, 2015, from http://www.un-redd.org/AboutREDD/tabid/102614/Default.aspx

Westerstad, C., 2011. Skogsvårdslagen och den biologiska mångfalden. Retrieved May 11th, 2015, from http://lup.lub.lu.se/luur/download?func=downloadFile&recordOId=3461019&fileOId=3461020

Zianis, D., P. Muukkonen, R. Mäkipää, and M. Mencuccini. 2005. Biomass and Stem Volume Equations for Tree Species in Europe. The Finnish Forest Research Institute. Retrieved March 13th, from http://www.metla.fi/silvafennica/full/smf/smf004.pdf

Appendix I

List of principles of the selective cutting system used at Romperöd, Glimåkra, Sweden (D. Göransson, personal communication, April 14th, 2015).

1. Cut primarily the biggest trees – especially while spruce should not reach a diameter (at breat-height), which exceeds 60 cm (maximum for debarking machinery). Normally this means that spruces bigger than 50 cm should not be left.
2. Trees of low timber quality and slow growing trees in the upper story should be removed. The quality and height of the remaining timber trees are improved and wil cause a future regeneration with improved hereditary characteristics for timber production.
3. Growth should primarily be focused on big and valueable trees, and it is not so important to improve growth in smaller trees by thinning in dense groups – the high density will improve timber quality.
4. Trees which are so small, that cutting will give no profit, should normally only be cut if they have so bad quality that they are not expected to develop into timber (will never be better than firewood).
5. Take the risk of wind felling into consideration – do not thin too much. The cutting should preferably not exceed 35 % of the standing volume. Leave trees, which are resistant to wind felling (especially pine), and avoid making large holes for t he west wind.
6. Keep a sufficient standing volume (at least 100 m3/ha, preferably 150 m3/ha or more) to maintain a high growth and to support regeneration. The ideal in the Southern part of Sweden is perhaps a standing volume of 300 m3/ha before cutting and a removal of 100 trees and 100 m3/ha (= 1 m^3/tree) every 10-20 years.
7. Try always to keep the forest floor in shadow, especially for the noon sun – this is especially very important for stands on dry ground. Shadow hinders grass and supports the regeneration and decreases the share of deciduous trees in the regeneration.
8. Implementing the above principles causes adequate regeneration – now or later – without any other measures.
9. Seedlings and young trees do not need any special assitance and no consideration – except careful harvesting - is needed when cutting in the upper story. Small damages caused when cutting the old trees, merely support a natural selection, which often is

wanted. Then a pre-commercial thinning in the young trees is not necessary. Spruce can grow for many years in shadow and will quickly respond to light with an increased growth. Damaged and broken tops normally don't result in low timber quality in the long run.

10. The selective cutting system normally only regenerates shadow-species as spruce. But heavy windfalls (expected to happen several times during a century) will occasionally result in regeneration of pine. If the selective cutting system should survive in a stand with a heavy windfall, it is important that the remaining old trees are not cut.

Appendix II

Table 4. Field measurements and AGB estimations.

Field plot	Dominant tree type	Tree count (No)	Tree density (No/ha)	Mean diameter (cm)	Diameter SD	Mean tree height (m)	Tree height SD	AGB (kg)	AGB (kg/ha)
N100	Spruce	31	1550	8.6	9.0	7.8	8.1	2418.4	120920.6
NE50	Spruce	19	950	16.2	14.6	12.3	9.1	3507.2	175358.4
NE90	Birch	32	1600	8.0	9.8	7.4	5.5	2012.7	100637.2
E50	Spruce	57	2850	7.3	7.0	7.4	6.2	2567.7	128386.5
E100	Spruce	33	1650	12.3	10.8	11.4	9.4	4816.7	240835.8
SE50	Spruce	20	1000	18.5	12.9	13.6	7.7	3809.3	190467.2
SE100	Spruce	44	2200	8.4	7.6	8.8	6.0	2698.1	134903.8
S50	Spruce	42	2100	13.1	7.4	13.6	6.9	4157.0	207847.6
S100	Birch	23	1150	15.0	14.1	12.7	8.7	4301.3	215062.7
SW50	Spruce	37	1850	12.8	9.5	11.1	6.5	3459.7	172986.3
SW100	Birch	24	1200	11.3	8.2	11.3	5.1	1770.7	88532.8
W50	Spruce/Birch	35	1750	9.6	3.7	9.8	4.5	1135.1	56756.5
W100	Spruce	27	1350	14.4	10.3	13.8	6.8	3601.2	180057.6
NW50	Spruce	27	1350	13.2	10.4	13.3	8.0	3085.7	154282.6
NW100	Spruce	24	1200	9.4	8.6	7.9	5.9	1395.8	69790.1
NW200	Birch	18	900	3.6	0.4	5.5	0.5	40.5	2023.5
NW325	Beech	8	400	27.7	13.7	21.1	9.0	5456.1	272805.9

SD is the standard deviation

Table 5. Accuracy assessment of DEMs.

Field plot	Reference elevation (m.a.s.l.)	DTM (m.a.s.l.)	Elevation deviation (m)	Reference mean tree height (m)	CHM (m)	Tree height deviation (m)
N100	86.6	86.3	0.3	7.8	13.2	-5.3
NE50	87.0	85.8	1.2	12.3	14.3	-2.0
NE90	86.3	85.0	1.3	7.4	14.4	-7.0
E50	87.3	85.9	1.4	7.4	11.9	-4.5
E100	85.8	85.4	0.4	11.4	12.3	-0.9
SE50	93.4	91.4	2.0	13.6	13.7	-0.1
SE100	97.1	89.9	7.2	8.8	8.4	0.4
S50	92.1	89.5	2.6	13.6	13.3	0.3
S100	92.2	91.5	0.7	12.7	11.9	0.8
SW50	87.3	89.8	-2.5	11.1	12.2	-1.1
SW100	96.6	93.1	3.5	11.3	10.5	0.8
W50	88.6	89.1	-0.5	9.8	6.5	3.3
W100	93.2	92.9	0.4	13.8	10.6	3.2
NW50	89.4	88.7	0.8	13.3	11.4	1.8
NW100	90.2	89.6	0.6	7.9	8.4	-0.6
NW200	101.5	101.1	0.4	5.5	0.6	4.9
NW325	99.2	99.3	-0.1	21.1	17.1	4.1

Appendix III

The attributes used in the classification can be seen in the tables below (ENVI, nd):

Table 6. Spectral attributes computed for the land cover classification.

Spectral Attribute	Description
Mean	Average value of the pixels compromising the region in band x
Max	Maximum value of the pixels comprising the region in band x
Min	Minimum value of the pixels comprising the region in band x
SD	Standard deviation value of the pixels comprising the region in band x

Table 7. Texture attributes computed for the land cover classification.

Texture Attribute	Description
Range	Average data range of pixels comprising the region inside the kernel.
Mean	Average value of the pixels comprising the region inside the kernel.
Variance	Average variance of the pixels comprising the region inside the kernel.
Entropy	Average entropy value of the pixels comprising the region inside the kernel.

Table 8. Spatial attributes computed for the land cover classification.

Spatial Attribute	Description
Area	Total area of the polygon, minus the area of the holes. If the input image is pixel-based, the area is the number of pixels in the segmented object.
Length	The combined length of all boundaries of the polygon, including the boundaries of the holes.
Compactness	A shape measure that indicates the compactness of a polygon. A circle is the most compact shape with a value of 1 / pi. The compactness value of a square is 1 / 2(sqrt(pi)).
Convexity	Polygons are either convex or concave. This attribute measures the convexity of the polygon. The convexity value for a convex polygon with no holes is 1.0, while the value for a concave polygon is less than 1.0. Convexity = length of convex hull / Length.
Solidity	A shape measure that compares the area of the polygon to the area of a convex hull surrounding the polygon. The solidity value for a convex polygon with no holes is 1.0, and the value for a concave polygon is less than 1.0. Solidity = Area / area of convex hull.

Roundness	A shape measure that compares the area of the polygon to the square of the maximum diameter of the polygon. The "maximum diameter" is the length of the major axis of an oriented bounding box enclosing the polygon. The roundness value for a circle is 1, and the value for a square is 4 / pi. Roundness = 4 * (Area) / (pi * Major_Length2)
Form factor	A shape measure that compares the area of the polygon to the square of the total perimeter. The form factor value of a circle is 1, and the value of a square is pi / 4. Form_Factor = 4 * pi * (Area) / (total perimeter)^2
Elongation	A shape measure that indicates the ratio of the major axis of the polygon to the minor axis of the polygon. The major and minor axes are derived from an oriented bounding box containing the polygon. The elongation value for a square is 1.0, and the value for a rectangle is greater than 1.0. Elongation = Major_Length / Minor_Length
Rectangular fit	A shape measure that indicates how well the shape is described by a rectangle. This attribute compares the area of the polygon to the area of the oriented bounding box enclosing the polygon. The rectangular fit value for a rectangle is 1.0, and the value for a non-rectangular shape is less than 1.0. Rectangular_Fit = Area / (Major_Length * Minor_Length)
Main direction	The angle subtended by the major axis of the polygon and the x-axis in degrees. The main direction value ranges from 0 to 180 degrees. 90 degrees is North/South, and 0 to 180 degrees is East/West.
Major length	The length of the major axis of an oriented bounding box enclosing the polygon. Values are map units of the pixel size. If the image is not georeferenced, then pixel units are reported.
Minor length	The length of the minor axis of an oriented bounding box enclosing the polygon. Values are map units of the pixel size. If the image is not georeferenced, then pixel units are reported.
Number of Holes	The number of holes in the polygon. Integer value.
Hole area/Solid area	The ratio of the total area of the polygon to the area of the outer contour of the polygon. The hole solid ratio value for a polygon with no holes is 1.0. Hole_Area/Solid_Area = Area / outer contour area

Institutionen för naturgeografi och ekosystemvetenskap, Lunds Universitet.

Student examensarbete (Seminarieuppsatser). Uppsatserna finns tillgängliga på institutionens geobibliotek, Sölvegatan 12, 223 62 LUND. Serien startade 1985. Hela listan och själva uppsatserna är även tillgängliga på LUP student papers (https://lup.lub.lu.se/student-papers/search/) och via Geobiblioteket (www.geobib.lu.se)

The student thesis reports are available at the Geo-Library, Department of Physical Geography and Ecosystem Science, University of Lund, Sölvegatan 12, S-223 62 Lund, Sweden. Report series started 1985. The complete list and electronic versions are also electronic available at the LUP student papers (https://lup.lub.lu.se/student-papers/search/) and through the Geo-library (www.geobib.lu.se)

335 Fei Lu (2015) Compute a Crowdedness Index on Historical GIS Data- A Case Study of Hög Parish, Sweden, 1812-1920

336 Lina Allesson (2015) Impact of photo-chemical processing of dissolved organic carbon on the bacterial respiratory quotient in aquatic ecosystems

337 Andreas Kiik (2015) Cartographic design of thematic polygons: a comparison using eye-movement metrics analysis

338 Iain Lednor (2015) Testing the robustness of the Plant Phenology Index to changes in temperature

339 Louise Bradshaw (2015) Submerged Landscapes - Locating Mesolithic settlements in Blekinge, Sweden

340 Elisabeth Maria Farrington (2015) The water crisis in Gaborone: Investigating the underlying factors resulting in the 'failure' of the Gaborone Dam, Botswana

341 Annie Forssblad (2015) Utvärdering av miljöersättning för odlingslandskapets värdefulla träd

342 Iris Behrens, Linn Gardell (2015) Water quality in Apac-, Mbale- & Lira district, Uganda - A field study evaluating problems and suitable solutions

343 Linnéa Larsson (2015) Analys av framtida översvämningsrisker i Malmö - En fallstudie av Castellums fastigheter

344 Ida Pettersson (2015) Comparing Ips Typographus and Dendroctonus ponderosas response to climate change with the use of phenology models

345 Frida Ulfves (2015) Classifying and Localizing Areas of Forest at Risk of Storm Damage in Kronoberg County

346 Alexander Nordström (2015) Förslag på dammar och skyddsområde med hjälp av GIS: En studie om löv- och klockgroda i Ystad kommun, Skåne

347 Samanah Seyedi-Shandiz (2015) Automatic Creation of Schematic Maps - A Case Study of the Railway Network at the Swedish Transport Administration

348 Johanna Andersson (2015) Heat Waves and their Impacts on Outdoor Workers – A Case Study in Northern and Eastern Uganda

349 Jimmie Carpman (2015) Spatially varying parameters in observed new particle formation events

350 Mihaela – Mariana Tudoran (2015) Occurrences of insect outbreaks in Sweden in relation to climatic parameters since 1850

351 Maria Gatzouras (2015) Assessment of trampling impact in Icelandic natural areas in experimental plots with focus on image analysis of digital photographs

352 Gustav Wallner (2015) Estimating and evaluating GPP in the Sahel using MSG/SEVIRI and MODIS satellite data

353 Luisa Teixeira (2015) Exploring the relationships between biodiversity and benthic habitat in the Primeiras and Segundas Protected Area, Mozambique

354 Iris Behrens & Linn Gardell (2015) Water quality in Apac-, Mbale- & Lira district, Uganda - A field study evaluating problems and suitable solutions

355 Viktoria Björklund (2015) Water quality in rivers affected by urbanization: A Case Study in Minas Gerais, Brazil

356 Tara Mellquist (2015) Hållbar dagvattenhantering i Stockholms stad - En riskhanteringsanalys med avseende på långsiktig hållbarhet av Stockholms stads

dagvattenhantering i urban miljö

357 Jenny Hansson (2015) Trafikrelaterade luftföroreningar vid förskolor – En studie om kvävedioxidhalter vid förskolor i Malmö

358 Laura Reinelt (2015) Modelling vegetation dynamics and carbon fluxes in a high Arctic mire

359 Emelie Linnéa Graham (2015) Atmospheric reactivity of cyclic ethers of relevance to biofuel combustion

360 Filippo Gualla (2015) Sun position and PV panels: a model to determine the best orientation

361 Joakim Lindberg (2015) Locating potential flood areas in an urban environment using remote sensing and GIS, case study Lund, Sweden

362 Georgios-Konstantinos Lagkas (2015) Analysis of NDVI variation and snowmelt around Zackenberg station, Greenland with comparison of ground data and remote sensing.

363 Carlos Arellano (2015) Production and Biodegradability of Dissolved Organic Carbon from Different Litter Sources

364 Sofia Valentin (2015) Do-It-Yourself Helium Balloon Aerial Photography - Developing a method in an agroforestry plantation, Lao PDR

365 Shirin Danehpash (2015) Evaluation of Standards and Techniques for Retrieval of Geospatial Raster Data - A study for the ICOS Carbon Portal

366 Linnea Jonsson (2015) Evaluation of pixel based and object based classification methods for land cover mapping with high spatial resolution satellite imagery, in the Amazonas, Brazil.

367 Johan Westin (2015) Quantification of a continuous-cover forest in Sweden using remote sensing techniques